Article:

Udeh, G.T., Michailos, S., Ingham, D. et al. (3 more authors) (2020) A new non-ideal second order thermal model with additional loss effects for simulating beta Stirling engines. Energy Conversion and Management, 206. 112493. ISSN 0196-8904

https://doi.org/10.1016/j.enconman.2020.112493

A new non-ideal second order thermal model with additional loss effects for simulating beta Stirling engines.

Godfrey T. Udeh[a,b*], Stavros Michailos[b], Derek Ingham[b], Kevin J. Hughes[b], Lin Ma[b], Mohammed Pourkashanian[b]

a. *Department of Mechanical Engineering, Faculty of Engineering, University of Port Harcourt, Nigeria.*

b. *Energy 2050, Department of Mechanical Engineering, University of Sheffield, Sheffield, S3 7RD, United Kingdom.*

Corresponding author: gtudeh1@sheffield.ac.uk

Abstract: In this paper, comprehensive governing differential equations of Stirling engines have been developed by coupling the effect of gas leakage through the displacer gap, gas leakage into the crank case and the shuttle loss rate into the traditional model. Instantaneous pressures and temperatures of the working fluid in the engine were evaluated at same time step. The present model was deployed for the thermal simulation of the GPU-3 Stirling engine and the obtained results were robustly compared to experimental data as well as results from previous numerical models. Then, parametric studies were conducted to assess the impact of geometrical and operating parameters on the performance of Stirling engines working with helium or hydrogen. Results suggest that the modifications made in this model led to better accuracy and consistency in predicting the experimental data of the prototype engine at all speeds, compared with most previous models. It was found that there exists a minimum dimensionless gap number, for every engine pressure below which mass leakage into the compression volume may not impact the brake power and energetic efficiency of the engine. In addition, an optimum mean effective pressure was found for maximum energetic efficiency of the engine. This optimum value is higher for helium gas than for hydrogen gas. Further results indicated that the brake power and energetic efficiency of the prototype Stirling engine can be significantly improved by 30% and 18%, respectively, provided that the heater temperature is raised to 850 °C while the cooler temperature is reduced to 0 °C.

Keywords: Stirling engine; Heat and mass leakage; Dimensionless gap number; Heater temperature; Cooler temperature; Energetic efficiency.

1. Introduction

The mounting environmental concerns associated with the use of fossil fuels is driving the increasing utilisation of renewable energy sources (RES), such as biomass, solar, wind, geothermal, for clean energy generation. In spite of this, fossil fuel fired internal combustion engines are still being deployed to guarantee the reliability of RES systems (especially in island mode operations), because of their intermittent nature [1–3]. Stirling engines pose a promising alternative to replace the internal combustion engines, mainly in decentralised applications, as they can utilise multiple clean low – medium grade thermal energy sources in their operation [4–7] and also, as a consequence of its high performance in combined heating and power (CHP) applications [8]. As a result, this external combustion engine which was invented over four decades before the invention of the diesel engine [9], is now attracting much research interest. Other interesting features of Stirling engines include ease of operation and construction, quietness in operation, low emissions and high part load performance [10–12]. Stirling engines, better known as regenerative thermal engines, utilise a regenerator to minimise the thermal energy needed by a conventional heat engine to produce its power, by about 80% [13]. Hence, the regenerator plays a crucial role in their operation, and contributes significantly to the complexity of the thermal analysis of the heat engine. In fact, several recent efforts have been made to improve on the performance of Stirling engines using new regenerator designs and matrix materials [14–16].

So far, the thermal analysis of Stirling engines have been undertaken using empirical, analytical and numerical models [17]. Furthermore, based on the depth of the analysis, the models deployed to predict the engine's performance are classified as zero order, first order, second order, third order and fourth order [18–20]. The zero order models are empirical models deploying experimental coefficients to predict the performance of the engine, whilst the first order models are mainly closed form analytical models [19]. The second, third and fourth order models on the other hand, are numerical models with increasing level of accuracy respectively, but requiring much computing time [20].

The preliminary design of Stirling engines have been undertaken using zero order models in the literature [21–26]. These authors deployed dimensionless numbers [21], and other empirical correlations to predict the performance of Stirling engines, mainly as a function of some of the operating variables of the engine including, cycle mean pressure, piston displacement volume, temperature ratio and the speed of the engine. The predicted results were useful in estimating the power output and First Law (energetic) efficiency of the experimental engine, for the range of operating parameters defined in developing the models. Regardless, the zero order models developed in the literature over predicts the performance of the experimental engine. Hence, these models are only suitable for the quick design of Stirling engines [23]. Other limitations of the zero order model are its inability to describe the detailed processes occurring in the engine, and relate the geometrical parameters of the engine to its performance.

Several analytical models are available in the open literature that simulate the performance of Stirling engines [27–31]. Schmidt [27] formulated the pioneer analytical model based on isothermal analysis, to simulate the behaviour of Stirling engines. He assumed isothermal conditions for the thermodynamic work processes in the engine. The Schmidt model could reveal the pressure distribution in the main components of the engine. Nonetheless, it overestimated the performance of the prototype engine (by 30 – 60%), since isothermal processes can only be achieved in practice using an infinite heat transfer surface. Martini [28] improved on the Schmidt model by coupling the internal irreversibilities in the regenerator and other heat exchangers, to the isothermal model. This model accounted for the imperfect regeneration and some of the heat losses in the engine. Other researchers deployed modelling tools based on classical thermodynamics, such as the finite-time thermodynamics (FTT) [29,30] and the finite-speed thermodynamics (FST) [32–36] to model the time-invariant performance of Stirling engines. The FST modelling approach gave better results than the FTT approach and this is because both internal and external irreversibilities were considered in the former while the latter only considered external irreversibilities. Although analytical models for predicting the performance of Stirling engines are usually easy to implement, reducing the complexity and the computational costs associated with higher order models [37], these models accuracy are limited because of the assumed isothermal processes. In addition, analytical models do not relate the engine's main design parameters to the engine's thermal performance metrics.

Second order modelling approach of Stirling engines was deployed for the first time by Finkelstein [38], based on isentropic work processes in the compression and expansion spaces of the engine. Urieli and Berchowitz [39] pioneered the development of a computer based code to implement the numerical solutions of the Finkelstein adiabatic model. Urieli and Berchowitz [39] further improved on the Finkelstein model by accounting for some irreversibilities in the engine, in what is called the Simple analysis. They divided the engine into five main control volumes, and conducted a mass and energy balance at the ingress and egress of these control volumes. The resulting differential equations, linking the engine's geometrical parameters and the physical properties of the internal gas to its thermal performance indicators, were solved using the fourth-order Runge-Kutta numerical scheme. Further efforts have been made to improve on the Urieli and Berchowitz [39] model by several other researchers, by accounting for other losses in the engine [40–43]. Timoumi et al. [40] improved on the Urieli and

Berchowitz [39] model by considering the losses due to energy dissipation in the engine, external conduction, internal conduction, shuttle effect and spring hysteresis in the engine, in their model. Their model results were more accurate than that of Urieli and Berchowitdz [39], and compares favourably with the model results presented by Martini [28]. In the Simple-II analysis [41], the prediction accuracy of the Simple analysis model [39] has been improved, by coupling the shuttle heat loss and mass leakage into the buffer space, to the differential equations modelling the engine. Furthermore, losses due to mechanical friction, variation in the working pressure around the piston, longitudinal conduction through the wall of the regenerator from thermal communication with the heater and cooler walls, were accounted for at the end of each cycle. Their model could predict the output power and energetic efficiency of the GPU-3 Stirling engine, with 20.7% and 7.1% errors (the difference between the model data and the experimental data), respectively. Babaelahi and Sayyaadi [42] developed the polytropic model with Stirling various losses (PSVL), to predict the performance of Stirling engines. As an improvement over the Simple-II model, this model replaced the adiabatic processes in the former with polytropic expansion and compression, and evaluated the polytropic exponents using the engine's operating parameters. They reported errors as a difference of 14.34% and 3.14% in predicting the power output and the energetic efficiency of the experimental engine, respectively. In another study, Babaelahi and Sayyaadi [43] improved on the accuracy of the PSVL model [42], by coupling the polytropic heat losses from the expansion and compression spaces, to the energy balance equations of those spaces. Other studies deploying the second order model have been reported in the literature [44–50].

Recently, Li et al. [51] improved on the existing models, by coupling the shuttle heat loss and mass leakage through the gap between the displacer and the cylinder wall, to the differential equations of the engine, while assuming that the compression and expansion processes were polytropic. In addition, by contrast to other second order models, Li et al. [51] introduced the internal and external irreversibilities of the engine to the model, in such a manner that they are accounted for in each time step and interact with each other. They reported that the mass leakage into the compression space via the displacer gap contributed the second largest work loss in the engine of 4.1%. Their model could predict the work rate and energetic efficiency of the GPU-3 Stirling engine with a relative error of – 2.6% and + 3.78%, respectively. They however, did not consider the dissipation of energy in the engine as a result of frictional effects, which would impact on the instantaneous pressure and temperature of the working fluid in the expansion and compression spaces, and in the heat exchangers of the engine, at each time step.

Consequently, this model just as in [36,42,43,48] predicted linear trends for the energetic efficiency of the GPU-3 Stirling engine at different engine rotational speeds.

The second order models of Stirling engines are suitable for conducting parametric studies on the engine. Notwithstanding, they do not give detailed information of the thermal and flow fields in the engine. In particular, these models do not reveal the velocity, temperature, density, and pressure profiles of the working fluid, at all points, in the control volumes of the engine [52]. To fully understand the flow behaviour in the working spaces of the engine, third and fourth order modelling approaches are usually deployed. Third order modelling involves formulating partial differential equations governing the operation of the engine, based on mass, momentum, and energy balances of the different control volumes. Toghyani et al. [53] deployed a third order model to determine the optimal heat source temperature, frequency, engine stroke and mean effective pressure of the GPU-3 Stirling, that would yield the maximum power output and energetic efficiency. They found that the fuzzy decision making method gave the best performance results out of the Pareto solutions. This model however, did not yield better results than the existing adiabatic models. This is because the authors over simplified the complex processes in the engine in order to increase the computing speed.

On the other hand, fourth order modelling involves deploying 3-D CFD technique to solve the complex flow problems taking place in the engine at every node of the mesh generated. Marek and Jan [54] deployed a dynamic mesh to map the various volumes of the Stirling engine in a 3-D CFD modelling study. The authors compared the results of the adiabatic models to that obtained from the fourth order modelling approach. They reported that the second order models are better for design and optimisation of the engine because of the shorter computational time. Mohammadi and Jafarian [55] deployed an open source CFD software (OpenFoam), to investigate the impact of hydrodynamic losses, on the performance of the Stirling engine. They reported an error of 15.15% in predicting the experimental engine's power output. Several other recent studies, where the thermal modelling of different configurations of Stirling engines using the 3-D CFD approach were implemented, have been reported in the literature [56–61]. Although the 3-D CFD analysis provided more insight about the flow fields in the engine, and the distribution of the losses, results obtained from this approach were not significantly better than that of existing second order models. This was attributed to the difficulty in representing the complex processes in the Stirling engine, in a CFD model. Moreover, CFD analyses consume much computing time compared to second order numerical analyses.

Therefore, we have enhanced the second order models for thermal analysis of Stirling engines to predict accurate and consistent performance results at all rotational speeds. So far, the existing second order models of the Stirling engine have failed to accurately match the experimental data with the predicted energetic efficiency and power at all speeds. Hence, in dynamic operation of the engine, where variation in its speed is inevitable, the results that are obtained using existing models may not reflect the engines actual performance.

To this end, a non-ideal thermal model with several loss effects has been proposed in this study. For the first time, a comprehensive modification of the traditional adiabatic model has been undertaken, by coupling the first category loss effects, including mass leakage through the displacer gap, mass leakage into the buffer space and shuttle conduction loss, into the simple adiabatic model. In addition, the instantaneous pressure and temperature of the working fluid in the control volumes were evaluated at each time step. Other second and third category loss effects such as dissipation loss, conduction loss, spring hysteresis loss, mechanical friction loss, piston finite speed loss, enthalpy leakage loss, regenerator imperfection loss, pressure drop in heat exchangers, are introduced into the numerical model results. This modelling approach has been implemented in MATLAB, and the solutions to the governing differential equations were obtained by the fourth-order Runge-Kutta numerical scheme approach. The obtained model results were validated against experimental data from the GPU-3 Stirling engine, and compared to results of other second order models. In addition, parametric studies were conducted to investigate the contribution of the heater temperature, cooler temperature, dimensionless gap number, and mean effective pressure on the performance of the engine, at different engine frequencies, using two working fluids: hydrogen and helium. This is intended to reveal the degree of impact these variables exert on the engine's performance, and suggest plausible ways to improve the performance of the engine.

2. Model formulation

Herein, the formulation of the thermodynamic models governing the operation of the Stirling engine, is presented, firstly based on the Urieli Simple analysis [39] and thereafter, the non-ideal thermal model is presented.

2.1. Simple adiabatic model

In the Simple analysis [39], Urieli and Berchowitz divided the Stirling engine into five main control volumes (CV), namely: heater, cooler, compression space, expansion space, and regenerator. They assumed that the thermodynamic work processes in the engine, occurred adiabatically. The other assumptions made in the Simple adiabatic analysis are as follows:

1. The thermodynamic processes in the engine attained steady state at the end of a cycle of its operation.
2. The engine is running at a constant speed.
3. A uniform instantaneous pressure in the working spaces of the engine.
4. The working fluid is treated as a perfect gas and obeys the ideal gas law.
5. The potential and kinetic energy of the working fluid exerts the same influence at the inlet and outlet of a control volume.
6. The total mass of the working fluid in the engine is invariant.
7. There is no mass leakage into the compression space from the working space via the cylinder wall-displacer gap.
8. There are no changes in the energy of the working fluid as a result of heat leakages between the working spaces or to the environment.
9. The heater and cooler are maintained at a constant temperature as it exchanges heat with the working fluid.

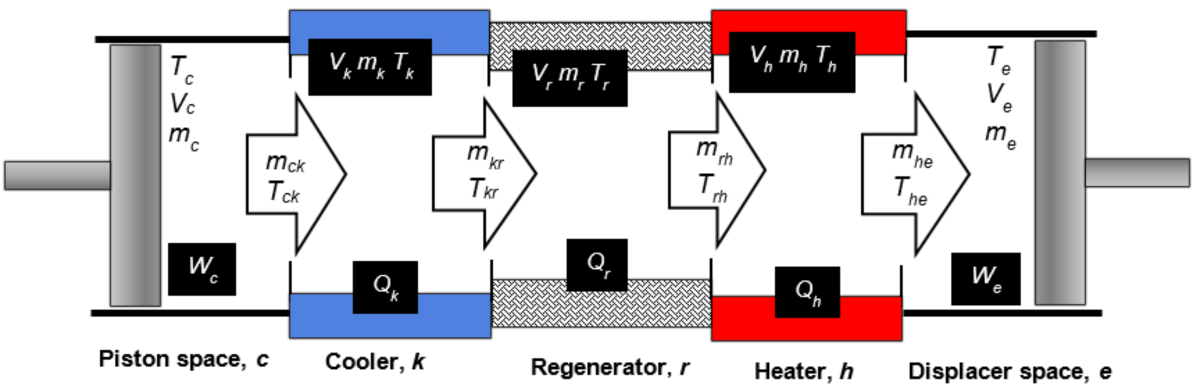

Fig. 1. Schematic diagram of the control volumes of a typical Stirling engine [39].

Urieli and Berchowitz [39] assigned single suffixes, *c, k, r, h, e* to represent the compression (cold) space, cooler, regenerator, heater and expansion (hot) space, respectively, while double suffices, *ck, kr, rh, he* represent the interfaces between the cold space – cooler, cooler – regenerator, regenerator – heater and heater – hot space, respectively as depicted in Fig. 1. The system of governing equations in the Simple analysis were derived by employing the equation of state of an ideal gas and the mass and energy conservation principles to each of the control volumes. These set of ordinary differential equations governing the operation of Stirling engines is summarized and presented in Table 1.

Table 1. Mass and energy balance equations of the Urieli adiabatic model [39].

$P = \frac{m_t R_g}{\left[\frac{V_c}{T_c} + \left(\frac{V_k}{T_k} + \frac{V_r}{T_r} + \frac{V_h}{T_h}\right) + \frac{V_e}{T_e}\right]}$	Pressure of the working fluid in the engine
$dP = \frac{-\gamma P\left(\frac{dV_c}{T_{ck}} + \frac{dV_e}{T_{he}}\right)}{\left[\frac{V_c}{T_c} + \gamma\left(\frac{V_k}{T_k} + \frac{V_r}{T_r} + \frac{V_h}{T_h}\right) + \frac{V_e}{T_e}\right]}$	Variation of pressure in the engine
$m_i = \frac{PV_i}{R_g T_i}, (i = c, k, r, h, e)$	Mass of working fluid in the engine's component
$dm_c = \frac{\left(PdV_c + \frac{V_c dp}{\gamma}\right)}{R_g T_{ck}}$	Change in the mass of working fluid
$dm_e = \frac{\left(PdV_e + \frac{V_e dp}{\gamma}\right)}{R_g T_{he}}$	
$dm_i = m_i \frac{dP}{P}, (i = c, k, r, h, e)$	
$dm_c = -m_{ck}$	Mass flow of working fluid
$dm_k = m_{ck} - m_{kr}$	
$dm_r = m_{kr} - m_{rh}$	
$dm_h = m_{rh} - m_{he}$	
$dm_e = m_{he}$	
$if\ m_{ck} > 0, T_{ck} = T_k; else\ T_{ck} = T_c$	Conditional temperature variation
$if\ m_{he} > 0, T_{he} = T_h; else\ T_{he} = T_e$	
$dT_i = T_i\left(\frac{dV_i}{V_i} + \frac{dP}{P} - \frac{dm_i}{m_i}\right), (i = c\ , e\ )$	Variation in the temperature in working spaces
$\partial Q_k = \frac{C_{vg}}{R_g} V_k\, dP + \left(C_{pg} T_{kr} dm_{kr} - C_{pg} T_{ck} dm_{ck}\right)$	Heat lost from cooler
$\partial Q_r = \frac{C_{vg}}{R_g} V_r\, dP + \left(C_{pg} T_{rh} dm_{rh} - C_{pg} T_{kr} dm_{kr}\right)$	Heat stored and released from regenerator
$\partial Q_h = \frac{C_{vg}}{R_g} V_h\, dP + \left(C_{pg} T_{he} dm_{he} - C_{pg} T_{rh} dm_{rh}\right)$	Heat gained in heater
$\partial W_e = p\, dV_e$	Expansion work done by displacer
$\partial W_c = p\, dV_c$	Compression work done by piston

2.2. New non-ideal thermal model with various losses

The proposed enhanced non-ideal thermal model of the Stirling engine with various losses has been developed in order to improve on the existing second order models deployed for thermal analysis of Stirling engines. Herein, the shuttle heat loss has been coupled into the energy flow equations of the hot and cold CVs in the engine, invalidating the adiabatic conditions assumed in the work processes in these CVs, made in the traditional model [39]. In addition, the mass leakage into the crankcase and the mass leakage into the cold CV were coupled into the mass conservation equations of the engine developed in [39], by considering the mass leakages across the boundaries of the CVs. These heat and mass losses that are coupled into the traditional equations form the first category losses [18,41,42]. With these modifications, the proposed model has been made more comprehensive by contrast to ref. [41–43] where only the mass leakage into the crankcase and shuttle conduction loss were coupled to the traditional equations. Also, compared with ref. [51] where only the mass leakage into the cold CV via the displacer gap and the shuttle heat loss were integrated into the traditional equations, the proposed model is more detailed. The resulting modified differential equations of the Stirling engine were solved using a fourth-order Runge-Kutta numerical scheme at each time step in every cycle.

In addition, the pressure drop in the heat exchangers of the engine was evaluated using empirical correlations and have been used to modify the instantaneous pressure and temperature of the working fluid in all of the components of the engine. At the end of each cycle, the second and third category loss effects were introduced into the already obtained numerical results to improve the results. The second category loss effects considered in this study which are mainly thermal losses are: loss due to regenerator imperfection, conduction loss, dissipation loss and enthalpy leakages to the buffer space. While the third category losses considered herein are work losses such as, pressure loss due to finite speed of the piston, mechanical frictional loss, spring hysteresis loss and loss due to pressure drop in the engine. The FST principle was used to model the pressure and mechanical frictional losses in the piston, with the assumption that the compression speed is equal to the expansion speed. Finally, the heater and cooler temperatures were corrected by conducting an energy balance of the components, assuming that the temperature of the heat source and sink are invariant.

In order to formulate the enhanced non-ideal thermal model then several of the assumptions in the ideal analysis have been discarded. The updated assumptions of the new enhanced non-ideal thermal model with various losses do not include the assumptions #3, #6, #7 and #8 of the Simple analysis [39], as cited and presented in Section 2.1.

2.2.1. Formulating the modified non-ideal thermal model

This model has been formulated by including additional compartments or control volumes (CV), to those presented in Fig. 1. Fig. 2 shows the additional CVs which are the gap between the displacer and the cylinder wall and that leading to the crankcase. The interface between the hot CV and the cold CV has been assigned suffix, *ce*, while *leak*, stands for the crankcase. The differential equations of the engine which are derivatives of the variables controlling the operation of the engine with respect to the crank angle (or time) were developed by conducting mass and energy balances of the CVs in the engine.

Neglecting the difference in the potential and kinetic heads in the flow energy equation (FEE), the generalized energy equation applicable to any of the CVs can be expressed as:

$$\begin{aligned}\{\delta Q_{\mathrm{ideal,j}} - \delta Q_{\mathrm{sh}} - \delta Q_{\mathrm{disp}} - \delta Q_{\mathrm{cond}} - \delta Q_{\mathrm{r,non-ideal}} - \delta Q_{\mathrm{leak}}\} \\ = \{(\dot{m}_{\mathrm{i}} c_{p,\mathrm{i}} T_{\mathrm{i}} - \dot{m}_{\mathrm{o}} c_{p,\mathrm{o}} T_{\mathrm{o}}) + \delta W_{\mathrm{ideal,j}} - \delta W_{\mathrm{mech.fric.}} - \delta W_{\mathrm{FST}} - \delta W_{\mathrm{hyst.}} \\ - \delta W_{\mathrm{pdrop}} + c_v d(mT)\}\end{aligned} \tag{1}$$

where $\delta Q_{\mathrm{ideal,j}}$ (W) is the ideal heat gained or lost and $\delta W_{\mathrm{ideal,j}}$ (W) the ideal work rate of the system (engine fluid) in any CV. The first and final terms on the right hand side of eq. (1) model the change in the energy content of the system in the CVs and its internal energy, with subscripts i and o standing for flow ingress and egress from the CV. Here, δQ_{sh} (J), δQ_{disp} (W), δQ_{cond} (W), $\delta Q_{\mathrm{r,non-ideal}}$ (W), and δQ_{leak} (W) are the additional terms to the traditional FEE namely the heat losses via the displacer shuttle, the energy dissipation, the conduction through the regenerator walls, the regenerator imperfection and the enthalpy leakage into the crank case respectively. In addition, $\delta W_{\mathrm{mech.fric.}}$ (W), δW_{FST} (W), $\delta W_{\mathrm{hyst.}}$ (W), and $\delta W_{\mathrm{pdrop}}$ (W) model the work loss rate via mechanical friction, the finite speed of the piston, the spring hysteresis and the pressure drop, respectively. c_p $\left(\frac{\mathrm{J}}{\mathrm{kg.K}}\right)$ and c_v $\left(\frac{\mathrm{J}}{\mathrm{kg.K}}\right)$ are the isobaric and isochoric specific heat capacities of the fluid, respectively.

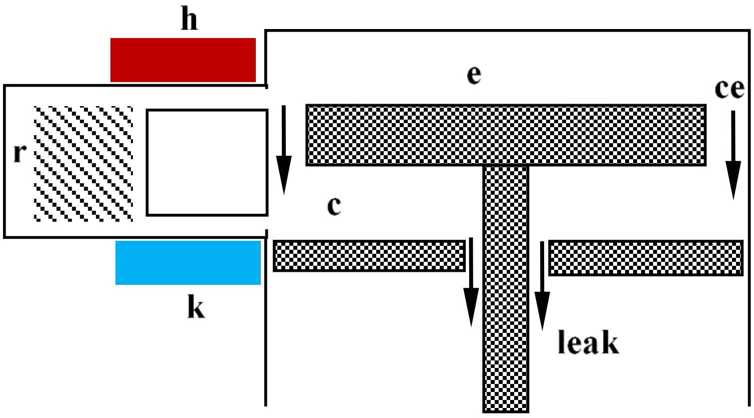

Fig. 2. Schematic of the beta type Stirling engine showing the mass leakage from the cylinder-displacer gap [51].

As the displacer travels from the cold CV to the hot CV, both maintained at two different temperature levels, there is some form of thermal communication between the displacer and the host volume during the process. The heat gained or lost by the displacer in the course of its movement between these two volumes is called the shuttle heat loss, and the instantaneous rate given by δQ_{sh}, has been modelled as [28,40]:

$$\delta Q_{\mathrm{sh}} = \frac{0.4 {Z_{\mathrm{d}}}^2 k_{\mathrm{d}} D_{\mathrm{d}}}{J_{\mathrm{d}} L_{\mathrm{d}}} (T_{\mathrm{e}} - T_{\mathrm{c}}) \tag{2}$$

where Z_{d} (m), k_{d} $(\frac{\mathrm{W}}{\mathrm{mk}})$, D_{d} (m), L_{d} (m), and J_{d} (m) are the displacer's stroke, thermal conductivity, diameter, length and annular gap between the displacer and the cylinder wall, respectively.

If only the shuttle heat loss and enthalpy leakage through the displacer clearance gap are considered in eq. (1), the energy balance of the compression CV and expansion CV will reduce to:

$$\delta Q_{\mathrm{c}} = -\delta Q_{\mathrm{sh}} + \frac{c_p}{R_{\mathrm{g}}} p dV_{\mathrm{c}} + \frac{c_v}{R_{\mathrm{g}}} V_{\mathrm{c}} dp + c_p T_{\mathrm{ck}} dm_{\mathrm{ck}} + c_p T_{\mathrm{ce}} dm_{\mathrm{ce}} \tag{3}$$

$$\delta Q_{\mathrm{e}} = \delta Q_{\mathrm{sh}} + \frac{c_p}{R_{\mathrm{g}}} p dV_{\mathrm{e}} + \frac{c_v}{R_{\mathrm{g}}} V_{\mathrm{e}} dp - c_p T_{\mathrm{he}} dm_{\mathrm{he}} - c_p T_{\mathrm{ce}} dm_{\mathrm{ce}} \tag{4}$$

where $R_{\mathrm{g}} \left(\frac{\mathrm{J}}{\mathrm{kg.K}}\right)$ is the gas constant of the working fluid.

Eqs. (3) and (4) were derived by noting that the shuttle heat is lost by the displacer (piston) in the compression volume and gained in the expansion volume. This is in line with the temperature gradient in these CVs. The last terms on the right hand side of these equations model the loss of enthalpy due to the mass leakage. As it can be seen, there would be a drop in the enthalpy in the hot CV and this is due to the mass leakage via the displacer gap which leads to a corresponding gain in enthalpy in the cold CV. Meanwhile, the mass of the working fluid that can escape from the expansion CV into the compression CV at any given time in the engine could be determined from the following expression [51,62]:

$$\dot{m}_{\mathrm{ce}} = \pi D_{\mathrm{d}} \frac{p}{4 R_{\mathrm{g}} T_{\mathrm{ce}}} \left(U_{\mathrm{d}} J_{\mathrm{d}} - \frac{J_{\mathrm{d}}^3}{6\mu_{\mathrm{g}}} \frac{\Delta p_{\mathrm{ce}}}{L_{\mathrm{d}}} \right) \tag{5}$$

where T_{ce} (K), U_{d} ($\frac{\mathrm{m}}{\mathrm{s}}$), μ_{g} ($\frac{\mathrm{Ns}}{\mathrm{m}^2}$), and Δp_{ce} (Pa) are the temperature of the fluid escaping through the displacer gap, velocity of the displacer, dynamic viscosity of the fluid and difference in pressure between the hot and the cold CVs, respectively.

The mass conservation principle has been applied to the spaces to obtain the rate of flow of the working fluid through each of the CVs are as follows:

$$dm_{\mathrm{ck}} = -dm_{\mathrm{c}} - dm_{\mathrm{ce}} \tag{6a}$$

$$dm_{\mathrm{kr}} = dm_{\mathrm{ck}} - dm_{\mathrm{k}} \tag{6b}$$

$$dm_{\mathrm{he}} = dm_{\mathrm{e}} - dm_{\mathrm{ce}} \tag{6c}$$

$$dm_{\mathrm{rh}} = dm_{\mathrm{he}} + dm_{\mathrm{h}} \tag{6d}$$

If eqs. (3), (4), (6a), and (6c) are combined and factorized, and noting that the compression and expansion processes are adiabatic, i.e. heat added (or lost) is zero, the rate of change of the mass of the working fluid in the cold and hot CVs is obtained as:

$$dm_{\mathrm{c}} = -\frac{\delta Q_{\mathrm{sh}} - \frac{c_p}{R_{\mathrm{g}}} p dV_{\mathrm{c}} - \frac{c_v}{R_{\mathrm{g}}} V_{\mathrm{c}} dp - c_p T_{\mathrm{ce}} dm_{\mathrm{ce}}}{c_p T_{ck}} - dm_{\mathrm{ce}} \tag{7}$$

$$dm_{\mathrm{e}} = \frac{\delta Q_{\mathrm{sh}} + \frac{c_p}{R_{\mathrm{g}}} p dV_e + \frac{c_v}{R_{\mathrm{g}}} V_{\mathrm{e}} dp - c_p T_{\mathrm{ce}} dm_{\mathrm{ce}}}{c_p T_{\mathrm{he}}} + dm_{\mathrm{ce}} \tag{8}$$

From the perfect gas equation, the instantaneous mass variation of the working fluid in the remaining CVs can be obtained from the following expression:

$$dm_{\mathrm{i}} = \frac{V_{\mathrm{i}}}{R_{\mathrm{g}} T_{\mathrm{i}}} dp, (\mathrm{i} = \mathrm{k}, \mathrm{r}, \mathrm{h}) \tag{9}$$

The instantaneous total amount of the working fluid in the engine is not expected to be constant because of the leakage of part of the gas into the crankcase. Thus, the amount of working fluid in the engine can be determined from the following expression:

$$m_{\mathrm{t}} = m_{\mathrm{c}} + m_{\mathrm{k}} + m_{\mathrm{r}} + m_{\mathrm{h}} + m_{\mathrm{e}} - m_{\mathrm{leak}} \tag{10}$$

where m_{leak} (kg) is the amount of the working fluid being lost from the cold CV of the engine into the crankcase.

The amount of working fluid lost from the engine into the crankcase per time is expressed as [39]:

$$\dot{m}_{\mathrm{leak}} = \pi D_{\mathrm{p}} \frac{p + p_{\mathrm{buffer}}}{4 R_{\mathrm{g}} T_{\mathrm{g}}} \left(U_{\mathrm{p}} J_{\mathrm{p}} - \frac{J_{\mathrm{p}}^3}{6 \mu_{\mathrm{g}}} \frac{p - p_{\mathrm{buffer}}}{L_{\mathrm{p}}} \right) \tag{11}$$

where U_{p} ($\frac{\mathrm{m}}{\mathrm{s}}$), p_{buffer} (Pa), D_{p} (m), L_{p} (m), and J_{p} (m) are the linear velocity of the piston, buffer pressure, piston diameter, length of piston and annular gap of the piston and the cylinder wall, respectively.

By differentiating eq. (10) and substituting eqs. (7), (8) and (9) into the resulting expression, the variation in the pressure of the working fluid is obtained as:

$$dp = \frac{\frac{\delta Q_{\mathrm{sh}} - \frac{c_p}{R_{\mathrm{g}}} p dV_{\mathrm{c}} - c_p T_{\mathrm{ce}} dm_{\mathrm{ce}}}{c_p T_{\mathrm{ck}}} - \frac{\delta Q_{\mathrm{sh}} + \frac{c_p}{R_{\mathrm{g}}} p dV_{\mathrm{e}} - c_p T_{\mathrm{ce}} dm_{\mathrm{ce}}}{c_p T_{\mathrm{he}}} + dm_{\mathrm{leak}}}{\frac{V_{\mathrm{c}}}{\gamma T_{\mathrm{ck}}} + \frac{V_{\mathrm{k}}}{T_{\mathrm{k}}} + \frac{V_{\mathrm{r}}}{T_{\mathrm{r}}} + \frac{V_{\mathrm{h}}}{T_{\mathrm{h}}} + \frac{V_{\mathrm{e}}}{\gamma T_{\mathrm{he}}}} R_{\mathrm{g}} \tag{12}$$

By coupling the mass leakage into the crankcase, the mass leakage through the annular displacer gap and the shuttle loss into the traditional differential equation of the Stirling engine, the eq. (12) has been formulated. In fact, eq. (12) encompasses the proposed novel modifications that have been made to the traditional model aiming to improve on the accuracy. Meanwhile, the instantaneous change in the temperature of the working fluid in the hot and cold CVs has been obtained from the ideal gas equation as follows:

$$dT_{\mathrm{i}} = T_{\mathrm{i}}\left(\frac{dV_{\mathrm{i}}}{V_{\mathrm{i}}} + \frac{dp}{p} - \frac{dm_{\mathrm{i}}}{m_{\mathrm{i}}}\right), \qquad i = c, e \tag{13}$$

Also, by conducting the energy balance of the heat exchangers in the Stirling engine using eq. (1), the quasi-ideal thermal energy exchange in the mentioned CVs was determined as:

$$\delta Q_{\mathrm{quasi-ideal,k}} = \frac{c_v}{R_{\mathrm{g}}} V_{\mathrm{k}} dp + c_p\big(T_{\mathrm{ck}}(dm_{\mathrm{c}} + dm_{\mathrm{ce}}) - T_{\mathrm{kr}}(dm_{\mathrm{c}} + dm_{\mathrm{ce}} + dm_{\mathrm{k}})\big) \tag{14}$$

$$\begin{aligned}\delta Q_{\mathrm{quasi-ideal,r}} = {} & \frac{c_v}{R_{\mathrm{g}}} V_{\mathrm{r}} dp \\ & + c_p T_{\mathrm{kr}}\big((dm_{\mathrm{c}} + dm_{\mathrm{ce}} + dm_{\mathrm{k}}) - T_{\mathrm{rh}}(dm_{\mathrm{c}} + dm_{\mathrm{ce}} + dm_{\mathrm{k}} + dm_{\mathrm{h}})\big)\end{aligned} \tag{15}$$

$$\delta Q_{\mathrm{quasi-ideal,h}} = \frac{c_v}{R_{\mathrm{g}}} V_{\mathrm{h}} dp + c_p\big(T_{\mathrm{rh}}(dm_{\mathrm{c}} + dm_{\mathrm{ce}} + dm_{\mathrm{k}} + dm_{\mathrm{h}}) - T_{\mathrm{he}}(-dm_{\mathrm{e}})\big) \tag{16}$$

The interfacial temperatures of the working fluid at the interfaces of the CVs have been determined by considering the direction of flow of the fluid. In this study, the interfacial temperatures of the fluid can be determined from the following expressions [51]:

$$\begin{gathered} if\ \dot{m}_{\mathrm{ck}} > 0, T_{\mathrm{ck}} = T_{\mathrm{k}} \\ else, T_{\mathrm{ck}} = T_{\mathrm{c}} \end{gathered} \tag{17}$$

$$\begin{gathered} if\ \dot{m}_{\mathrm{ce}} > 0, T_{\mathrm{ce}} = T_{\mathrm{c}} \\ else, T_{\mathrm{ce}} = T_{\mathrm{e}} \end{gathered} \tag{18}$$

$$\begin{gathered} if\ \dot{m}_{\mathrm{kr}} > 0, T_{\mathrm{kr}} = T_{\mathrm{k}} \\ else, T_{\mathrm{kr}} = T_{\mathrm{k}} + (1 - \varepsilon_{\mathrm{r}})(T_{\mathrm{h}} - T_{\mathrm{k}}) \end{gathered} \tag{19}$$

$$\begin{gathered} if\ m_{\mathrm{rh}} > 0, T_{\mathrm{rh}} = T_{\mathrm{h}} - (1 - \varepsilon_{\mathrm{r}})(T_{\mathrm{h}} - T_{\mathrm{k}}) \\ else, T_{\mathrm{rh}} = T_{\mathrm{h}} \end{gathered} \tag{20}$$

$$\begin{gathered} if\ \dot{m}_{\mathrm{he}} > 0, T_{\mathrm{he}} = T_{\mathrm{h}} \\ else, T_{\mathrm{he}} = T_{\mathrm{e}} \end{gathered} \tag{21}$$

The other modifications made to the Simple adiabatic analysis model in this study, to improve on those of ref. [43,51] is to implement the variation of pressure in the CVs of the engine using the magnitudes of the pressure drops in the heat exchangers. As in [40], the cold CV has been chosen as the reference pressure and assigned the value of the instantaneous pressure in the engine at a given time step. Subsequently, the pressure in the other components in a particular time step was determined incrementally by utilizing the information of the pressure drops in the heat exchangers in the previous time step and the direction of flow of the fluid, as follows:

$$if\ \dot{m}_{\mathrm{ck}} > 0, p_{\mathrm{k(i)}} = p_{\mathrm{c(i)}} + \frac{\Delta p_{\mathrm{k(i-1)}}}{2}$$
$$else, p_{\mathrm{k(i)}} = p_{\mathrm{c(i)}} - \frac{\Delta p_{\mathrm{k(i-1)}}}{2} \tag{22}$$

$$if\ \dot{m}_{\mathrm{kr}} > 0, p_{\mathrm{r(i)}} = p_{\mathrm{k(i)}} + \frac{\left(\Delta p_{\mathrm{k(i-1)}} + \Delta p_{\mathrm{r(i-1)}}\right)}{2}$$
$$else, p_{\mathrm{r(i)}} = p_{\mathrm{k(i)}} - \frac{\left(\Delta p_{\mathrm{k(i-1)}} + \Delta p_{\mathrm{r(i-1)}}\right)}{2} \tag{23}$$

$$if\ m_{\mathrm{rh}} > 0, p_{\mathrm{h(i)}} = p_{\mathrm{r(i)}} + \frac{\left(\Delta p_{\mathrm{r(i-1)}} + \Delta p_{\mathrm{h(i-1)}}\right)}{2}$$
$$else, p_{\mathrm{h(i)}} = p_{\mathrm{r(i)}} - \frac{\left(\Delta p_{\mathrm{r(i-1)}} + \Delta p_{\mathrm{h(i-1)}}\right)}{2} \tag{24}$$

$$if\ \dot{m}_{\mathrm{he}} > 0, p_{\mathrm{e(i)}} = p_{\mathrm{h(i)}} + \frac{\Delta p_{\mathrm{h(i-1)}}}{2}$$
$$else, p_{\mathrm{e(i)}} = p_{\mathrm{h(i)}} - \frac{\Delta p_{h(i-1)}}{2} \tag{25}$$

With the knowledge of the pressure of the fluid in each CV provided by eqs. (22) - (25), the temperature of the fluid in these CVs is updated in each time step by applying the following expression:

$$T_{\mathrm{i}} = \frac{p_{\mathrm{i}} V_{\mathrm{i}}}{R_{\mathrm{g}} m_{\mathrm{i}}}, (i = c, k, r, h, e) \tag{26}$$

These set of independent differential equations formulated for the analysis of Stirling engines can be presented as an initial value problem as follows:

$$\dot{y} = F(t, y), \qquad with\ initial\ conditions, y\left(t_{(0)}\right) = y_{(0)} \tag{27}$$

where, the array $y \equiv V_{\mathrm{c}}, V_{\mathrm{e}}, T_{\mathrm{c}}, T_{\mathrm{e}}, P, W_{\mathrm{c}}, W_{\mathrm{e}}, etc.$, denotes the unknown functions.

2.2.2. Modelling the second and third category losses in the engine

As stated in Section 2.2, the second and the third category losses of Stirling engines were accounted for in the enhanced non-ideal thermal model presented in this paper at the end of each cycle of the numerical iterations. The second and third category losses, as defined in the Section 2.2.1, have been incorporated into eq. (1). This section presents the principles and methods deployed in the evaluation of these losses.

2.2.2.1. Thermal losses in the enhanced Second-order modelling of the Stirling engine

The second category losses of the engine are mainly thermal losses. The thermal losses considered in this model are as follows:

a. Dissipation losses:

The flow of the working fluid over the walls of the heat exchangers of the Stirling engine creates a thermal boundary layer. This, in turn, induces heat dissipation which results in thermal losses. In this paper, this loss has been modelled by expressing it as a function of the pressure drops in the heat exchangers [39,40]:

$$Q_{\mathrm{diss,i}} = -\frac{\Delta p_{\mathrm{i}} m_{\mathrm{i}}}{\rho_{\mathrm{g}}}, (i = k, r, h) \tag{28}$$

where Δp_{i} (Pa) is the pressure drop in a given heat exchanger and ρ_{g} $(\frac{\mathrm{m}^3}{\mathrm{kg}})$ is the density of the internal gas of the engine.

b. Conduction losses:

The regenerative thermal engine utilises several heat exchangers, resulting in a variation in the temperature field across the engine. Some of the CVs are maintained at a high temperature, while others operate at a very low temperature. This obvious temperature differential can induce loss of thermal energy by internal conduction. In particular, a considerable amount of heat can be lost between the heater and the cooler - the units of the engine that operate at the extreme temperatures - as well as through the walls of the regenerator. This heat loss by internal conduction through the walls of the regenerator has been expressed as [44]:

$$Q_{\mathrm{cond}} = R_{\mathrm{cond}}(T_{\mathrm{wh}} - T_{\mathrm{wk}}) \tag{29}$$

where $R_{\mathrm{cond}} \left(\frac{\mathrm{kJ}}{\mathrm{K}}\right)$ is the conductive thermal resistance of the walls of the regenerator, T_{wh}(K) is the temperature of the heater wall and T_{wk} (K) is the temperature of the cooler wall.

c. Heat leakage to the buffer space:

The mass leakage into the crankcase could induce some thermal energy loss in the engine. This loss affects the performance of the engine. In Section 2.2.1, the mass of the compressed gas escaping into the buffer space was modelled. The enthalpy loss as a result of the mass leakage has been obtained as follows:

$$Q_{\mathrm{leak}} = m_{\mathrm{leak}} c_p T_{\mathrm{c}} \tag{30}$$

d. Non-ideal heat transfer losses:

It has been mentioned in Section 1, that the introduction of the regenerator in the Stirling engine could reduce the thermal energy requirement of the engine significantly. The regenerator is designed to absorb heat contained in the working fluid and to release ideally the same amount of heat when it is needed. Nevertheless, because of its thermal imperfections, it is impracticable to recover all of the heat absorbed. Hence, the performance of the regenerator is usually evaluated by its effectiveness, which simply expresses the fraction of the heat absorbed from the regenerator that could be recovered for a given regenerator design and operating conditions.

An effectiveness of 1.0 is the best case and implies complete heat recovery while 0.0 is the worst case indicating that no heat was recovered from the regenerator. It is unlikely to have an effectiveness of 1.0 in the regenerator, suggesting that the temperature of the working fluid exiting the regenerator is lower than the heater temperature. As a result, additional heat is supplied from the heater so as to make-up for the inefficiency of the regenerator and raise the fluid temperature to the required heater temperature. This however, comes at a cost; the reduction in the energetic efficiency of the engine. In this paper, the effectiveness of the regenerator was obtained using the number of transfer units (NTU) approach, with the help of empirical correlations. Thus, the effectiveness of the regenerator is taken herein as:

$$\varepsilon_{\mathrm{r}} = \frac{NTU}{NTU + 1} \tag{31}$$

The NTU is expressed as a function of the Nusselt number (Nu) of the matrix over which the fluid is flowing, and is expressed as [13]:

$$NTU = \left(\frac{4Nu}{RePr}\right)\frac{l_{\mathrm{r}}}{d_{\mathrm{hr}}} \tag{32}$$

where l_{r} (m), d_{hr} (m), Re (-) and Pr (-) are the length of the regenerator, hydraulic diameter of the regenerator, Reynolds and Prandtl numbers, respectively. The hydraulic diameter, d_{hr} which expresses the ratio of the void volume to that of the wetted area in the regenerator is given as:

$$d_{\mathrm{hr}} = \frac{4V_{\mathrm{void,r}}}{A_{\mathrm{wetted,r}}} \tag{33}$$

Geodon and Wood [25] studied the oscillating flows through the regenerator matrix and proposed for the estimation of the Nusselt number the following expression:

$$Nu = (1 + 0.99(RePr)^{0.66})\phi^{1.79} \tag{34}$$

where ϕ (-) is the porosity in the wire meshes contained in the regenerator and it can be expressed as [63]:

$$\phi = \frac{1 - (n_{\mathrm{mr}}\pi d_{\mathrm{wr}})}{4} \tag{35}$$

where d_{wr} (m), and n_{mr} ($\frac{1}{\mathrm{m}}$) are the regenerator mesh wire diameter and the number of meshes per meter, respectively.

Thus, the additional heat supplied by the heater to compensate for the regenerator imperfection has been obtained from:

$$Q_{\mathrm{r,non-ideal}} = Q_{\mathrm{r,ideal}}(1 - \varepsilon_{\mathrm{r}}) \tag{36}$$

The actual thermal load of the heater and the cooler have been obtained by incorporating the thermal losses modelled so far into their energy balance equations. These loads can, therefore, be obtained from the following expressions:

$$Q_{\mathrm{actual,k}} = Q_{\mathrm{quasi-ideal,k}} + Q_{\mathrm{cond}} - Q_{\mathrm{r,non-ideal}} + Q_{\mathrm{leak}} + Q_{\mathrm{diss,total}} \tag{37}$$

$$Q_{\mathrm{actual,h}} = Q_{\mathrm{quasi-ideal,h}} - Q_{\mathrm{cond}} + Q_{\mathrm{r,non-ideal}} - Q_{\mathrm{leak}} - Q_{\mathrm{diss,total}} \tag{38}$$

Then, eqs. (37) and (38) have been used to update the temperature of the cooler and the heater, at the end of each cycle, by deploying the Newton's law of cooling/heating, as expressed in the following relations [42]:

$$T_{\mathrm{h}} = T_{\mathrm{wh}} - \frac{\mathrm{Q}_{\mathrm{actual,h}} Freq}{h_{\mathrm{h}} A_{wh}} \tag{39}$$

$$T_{\mathrm{k}} = T_{\mathrm{wk}} - \frac{Q_{\mathrm{actual,k}} Freq}{h_{\mathrm{k}} A_{\mathrm{wk}}} \tag{40}$$

where $h_{\mathrm{h}}(\frac{\mathrm{W}}{\mathrm{m^2K}})$, $h_{\mathrm{k}}(\frac{\mathrm{W}}{\mathrm{m^2K}})$, $Freq$ (Hz), $A_{\mathrm{wh}}(\mathrm{m^2})$, and $A_{\mathrm{wk}}(\mathrm{m^2})$, are the heat transfer coefficients in the heater and cooler, the frequency of the engine, the area of the heater wall and the area of the cooler wall, respectively.

The heat transfer coefficients of the heater and cooler has been obtained from correlations in the literature [51] as:

$$h_{\mathrm{i}} = \frac{0.0791 \mu_{\mathrm{i}} c_p {Re_{\mathrm{i}}}^{0.75}}{2 D_{\mathrm{i}} Pr_{\mathrm{i}}}, (i = k, h) \tag{41}$$

2.2.2.2.Work transfer losses in the enhanced engine model

The work transfer losses have been described as third category losses in the Stirling engine [41,42], which inadvertently reduce the actual power generated by the engine. These losses are:

a. Loss of work due to drop in pressure in the exchangers:

The internal gas flowing through the cooler, heater and regenerator of the engine is in direct contact with the walls. Thanks to no slip condition at the fluid-wall interface, there is variation in the flow velocity and by extension, the pressure of the working fluid. The change in the pressure of the working fluid in the line of flow is responsible for the pressure loss in the heat exchangers of the Stirling engine, which affects its performance negatively. Thus, the pressure loss in the heat exchangers of the engine have been obtained in this paper as:

$$\Delta p_{\mathrm{i}} = \frac{2 f_{\mathrm{i}} \mu_{\mathrm{i}} u_{\mathrm{i}} V_{\mathrm{i}}}{d_{\mathrm{hi}}^{2} A_{\mathrm{i}}}, (i = k, h, r) \tag{42}$$

where u $(\frac{\mathrm{m}}{\mathrm{s}})$, A (m^2), and f (-) are the flow velocity, area of the heat exchanger and friction factor, respectively.

The frictional factor used in this paper has been obtained from empirical correlations, based on the flow regime of the flowing fluid in the heat exchanger and can be expressed as [39]:

$$f_{\mathrm{i}} = \begin{cases} 16 & Re < 2000 \\ 7.343 \times 10^{-4} Re^{1.3142} & 2000 < Re < 4000 \\ 0.0791 Re^{0.75} & Re > 4000 \end{cases}, (i = k, h) \tag{43}$$

While the friction factor of the regenerator has been evaluated from the correlations given by Kay and Londons [64] as:

$$f_{\mathrm{r}} = 54 + 1.43 Re^{0.78} \tag{44}$$

The work loss as a result of the pressure drop in the aforementioned heat exchangers can be obtained from the following expression:

$$W_{\mathrm{pdrop}} = \oint \sum_{i=k,r,h} \Delta p_{\mathrm{i}} \, dV_{\mathrm{e}} \tag{45}$$

Finally, the pressure difference between the hot and the cold CVs of the Stirling engine, required to model the mass leakage through the annular gap, is described in eq.(5) and it is given as the sum of the pressure drops in the heat exchangers of the engine [51]:

$$\Delta p_{\mathrm{ce}} = p_{\mathrm{e}} - p_{\mathrm{c}} = \sum_{i=k,r,h} \Delta p_{\mathrm{i}} \tag{46}$$

b. Frictional work loss in the engine:

As the displacer compresses the internal gas of the engine, the pressure of the fluid around the displacer grows to a value higher than the average pressure of the working fluid in the engine, which reverses in the expansion process. Consequently, more compression work is produced in the actual engine operation than the ideal compression work. Likewise, in the expansion process of the prototype engine, less work is produced compared with the ideal expansion work because of the lower pressure around the piston during this process. Hence, the net-work output of the prototype engine would be less than that of the theoretical engine.

This loss of work in the engine, by reason of the finite motion of the piston, has been modelled by the principle of finite speed thermodynamics formulated by Petrescu [35].

On the other hand, there would be mechanical losses in the bearings and other mechanical joints of the engine. The combined finite speed and mechanical losses from the Stirling engine was obtained from the following expression [35]:

$$W_{\mathrm{FST\,\&\,mech\,fric}} = \int P_{\mathrm{cylinder}} \left(\pm \frac{\sqrt{3\gamma} u_{\mathrm{p}}}{c} \pm \frac{\Delta p_{\mathrm{f}}}{P_{\mathrm{cylinder}}} \right) dV \tag{47}$$

where c $(\frac{\mathrm{m}}{\mathrm{s}})$, Δp_{f} (Pa), and u_{p} $(\frac{\mathrm{m}}{\mathrm{s}})$ are the speed of the wave induced in the working fluid by the motion of the piston, the pressure drop as a result of mechanical friction and piston speed, respectively. It is important to note that the sign (+) was used in the compression process and (-) in the expansion process.

The following expressions have been used to obtain the values of c and Δp_{f} [41]:

$$c = \sqrt{\gamma R_{\mathrm{g}} T} \tag{48}$$

$$\Delta p_{\mathrm{f}} = 0.97 + 0.15 \frac{N_{\mathrm{r}}}{1000} \tag{49}$$

where N_{r} (rpm) is the rotational speed of the engine.

c. Work loss due to gas spring hysteresis caused by the motion of the displacer:

As the displacer compresses and expands the internal gas of the engine, it is likely that this internal gas could begin to act as a spring. This unusual behavior of the working fluid may introduce additional losses in the engine that could be in the form of the dissipation of the internal energy of the fluid. The dissipation loss, as a result of the gas spring hysteresis, has been modelled using the following expression [39]:

$$\dot{W}_{\mathrm{Hyst}} = \sqrt{\frac{1}{32} \omega \gamma^3 (\gamma - 1) T_{\mathrm{w}} p_{\mathrm{mean}} k_{\mathrm{g}}} \left(\frac{V_{\mathrm{d}}}{2V_{\mathrm{T}}} \right)^2 A_{wetted} \tag{50}$$

where ω $(\frac{\mathrm{rad}}{\mathrm{s}})$, k_{g} $(\frac{\mathrm{W}}{\mathrm{mk}})$, V_{d} (m^3), V_{T} (m^3), A_{wetted} (m^2) are the angular speed of the piston, the thermal conductivity of the gas, the instantaneous swept volume of the displacer, the total volume in the working volumes of the engine and the wetted area in the working space, respectively.

Thus, the brake power of the engine has been obtained by subtracting the work losses from the ideal work:

$$\dot{W}_{\text{actual}} = \left\{ \left\{ \oint (p_{\text{e}} dV_{\text{e}} + p_{\text{c}} dV_{\text{c}}) \right\} - W_{\text{FST \& mech fric}} - W_{\text{pdrop}} \right\} Freq - W_{\text{Hyst}} \tag{51}$$

Thus, the actual energetic efficiency of the Stirling engine is, given as:

$$\eta_{\text{Stirling}} = \frac{\dot{W}_{\text{actual}}}{Q_{\text{actual,h}} \cdot freq} \tag{52}$$

3. Model solution algorithm

In this section, an algorithm was developed to describe the approach for implementing the solutions of the set of governing differential equations formulated in Section 2. Fig. 3 describes the algorithm developed to implement the solutions. As it has been mentioned previously, the fourth-order Runge-Kutta numerical scheme has been deployed in solving the modified differential equations formulated in this paper. Prior to deploying the numerical scheme, as it is seen from the algorithm, analytical models based on the driving mechanism and engine configuration have been used to obtain the magnitudes of the volumes of the gas in the working spaces and its derivatives, V_{c}, V_{e}, dV_{c}, and dV_{e} as a function of crank angle (or time of operation of the engine) in one cycle of operation, which is expected to span from $\theta = 0^{\circ}$ to $\theta = 360^{\circ}$.

Other design parameters of the engine, such as the volumes of the cooler, heater and regenerator, V_{k}, V_{h}, and V_{r}, respectively, were obtained using physical measurements of the geometry of the prototype engine. Initial conditions of the temperatures of the working fluid in the heater and cooler were specified, while the gas temperature in the regenerator has been obtained as the effective mean of the heater and cooler temperatures [39]. Furthermore, initial conditions of the mass of the fluid were assumed, while the Schmidt's model has been deployed to obtain the initial mass of the fluid in the CVs of the engine. The fluid in the hot and cold CVs have been assigned the magnitudes of the heater and the cooler temperatures, respectively, at time, $t_{(0)}$. In addition, ten boundary conditions of the interfacial temperatures of the CVs were specified. In this solution approach, with the exception of variables used to determine constants and other engine geometrical properties, the size of the vector y denoting the unknown functions is 44, comprising the analytical variables and derivatives.

The magnitudes of seven of these variables (Q_{k}, Q_{h}, Q_{r}, W_{c}, W_{e}, T_{c}, and T_{e}) have been obtained by numerical integration, using the fourth-order Runge-Kutta scheme, while the remaining were determined analytically. This initial value problem was solved at each time step up to the maximum time step (in this case 1000), completing one cycle of operation of the engine, before it was tested for convergence. The convergence criteria specified require that the magnitudes of the temperature of the fluid in the cold and hot CVs in conjunction with the mean pressure of the engine at the beginning of the cycle, $t_{(0)}$ $(or\ \theta = 0^{\circ})$ should be equal to that at the end of the cycle, $t_{(1000)}$ $(or\ \theta = 360^{\circ})$. Until this condition is met, which implies that the system had attained steady steady, the differential equations were solved over repeated cycles, and the numerical results for each variable was logged in each time step. The solutions to the unknown functions, y provided in this step, have the form of a 2-dimensional array of size (44×1000). The processes described so far in this step is similar to that employed in the Simple analysis [39], except for the fact that the traditional differential equations of the Stirling engine cited in Table 1 have been modified as described in Section 2.2.

At the completion of each cycle, the numerical results were modified by accounting for the thermal and the work transfer loss effects in the engine, as discussed in Section 2.2.2, to obtain the actual work and the heat interactions in the engine, and compute its energetic efficiency. Subsequently, the magnitudes of the temperature of the internal gas of the engine in the heater and cooler were modified, as described in Section 2.2.2.1, using the computed heat transfer rate in the referenced engine spaces. Finally, the updated values of the temperature of the internal gas of the engine in the heater and the cooler were transferred to the next cycle to repeat the steps described until steady state is attained.

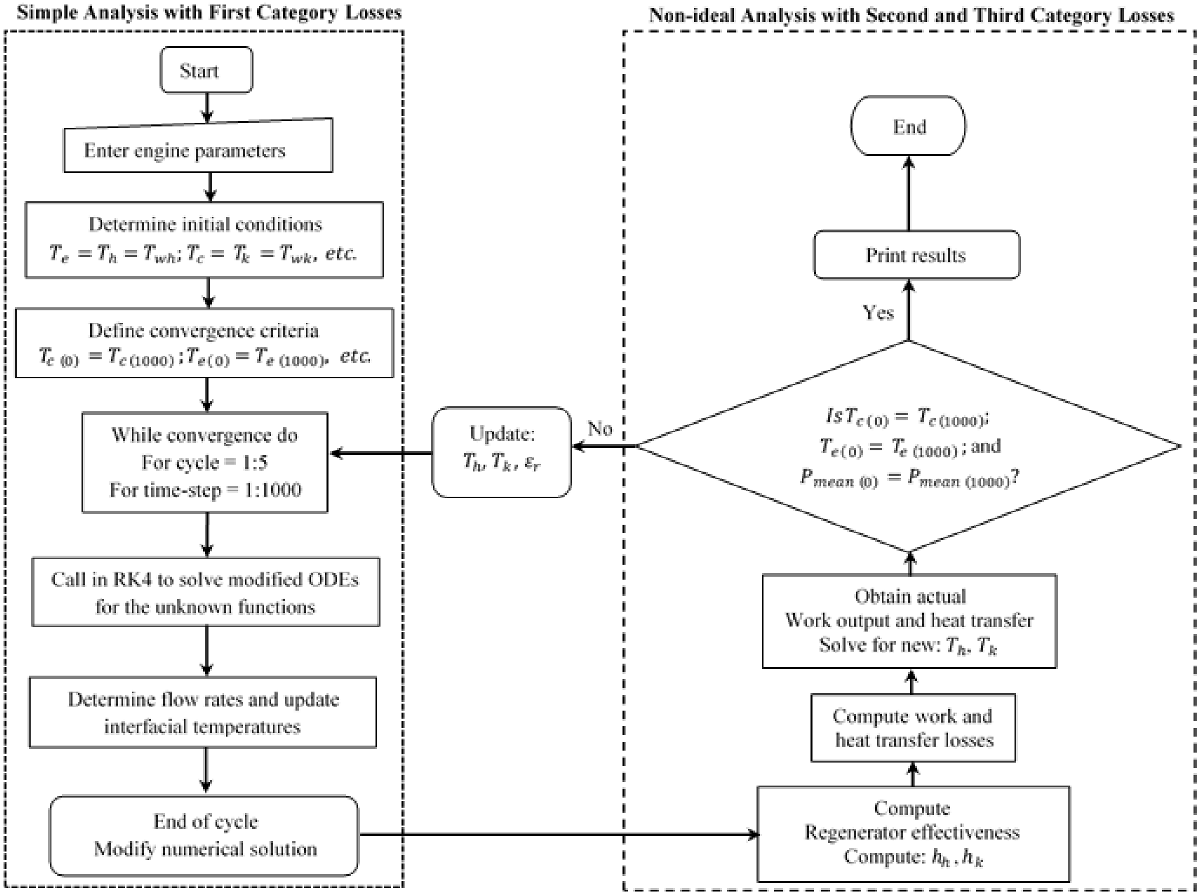

Fig. 3. Schematic of the solution algorithm deployed for analysing the proposed thermal model of the Stirling engine.

4. Enhanced model validation

The enhanced thermal model of the Stirling engine developed in this paper was evaluated with geometric and operating data of a 3 kW beta-type Stirling engine known as the GPU-3 Stirling engine and designed by General Motors. The testing of the GPU-3 Stirling engine was conducted in the NASA Lewis Research Center and the test results of the engine's performance was presented in [28]. The specifications of the geometrical design of the prototype engine are presented in Table 2.

Subsequently, the enhanced model formulated in this paper was validated against the test data from the GPU-3 Stirling engine and compared with model results developed in previous studies [36,39,41,42,48,51]. As depicted in Fig. 4 and Table 3 the enhanced model predicted the First Law efficiency and brake power of the prototype engine at the referenced point to a high level of accuracy with relative errors of + 0.3% and - 4.02% in the brake power and energetic efficiency, respectively. The high level of accuracy of the present model is a result of a deliberate effort to minimise the assumptions made in developing the model; hence, creating a more practical scenario.

Table 2. Design parameters of the prototype 3 kW Stirling engine [28] .

Quantity	Value	Quantity	Value
General		**Heater**	
Working fluid	Helium	Mean tube length	245.30 mm
Piston stroke	31.20 mm	Tube outside diameter	4.83 mm
Internal diameter of cylinder	69.90 mm	Tube inside diameter	3.02 mm
Frequency	41.70 Hz	Number of tubes per cylinder	40
Mean Pressure	4.13 MPa	Dead volume of heater	70.88 mm^3
Phase angle	90	**Cooler**	
Heater temperature	977 K	Mean tube length	46.10 mm
Cooler temperature	288 K	Tube external diameter	1.59 mm
Number of cylinder	1	Tube internal diameter	1.09 mm
Regenerator		Number of tubes per cylinder	312
Regenerator length	226 mm	Dead volume of cooler	13.80 mm^3
Regenerator external diameter	80 mm	**Others**	
Regenerator internal diameter	22.60 mm	Clearance volume of the piston	28.68 mm^3
Number of regenerator	8	Clearance volume of the displacer	30.52 mm^3
Dead volume of regenerator	50.55 mm^3	Diameter of displacer	69.9 mm
Material	Stainless steel wire	Diameter of displacer rod	9.52 mm
No. of wires per cm	79 × 79	Diameter of piston rod	22.2 mm
Wire diameter	0.04 mm	Displacer clearance	0.028 mm
No of layers	308	Piston clearance	0.15 mm
Porosity of the regenerator matrix	0.69	Eccentricity	20.80 mm

Meanwhile, in Fig. 4 and Table 3, the results obtained from the enhanced model, referred hereinafter as ‘Present Model’, have been compared to the results obtained from the models developed by: Urieli and Berchowitdtz [39], referred to as ‘Simple’; Babaelahi and Sayyaadi [41], referred to as ‘Simple II’; Sayyaadi and Hosseinzade [48], referred to as ‘CAFS’; Hosseinzade et al. [36], referred to as ‘PFST’; Babaelahi and Sayyaadi [42], referred to as ‘PSVL’; and Li et al. [51], thereafter referred to as ‘PSML’. These models are second order numerical models apart from the ‘PFST’ that is a closed-form model. By contrast to the previous models, the Present Model predicted superior results for both the brake power and the energetic efficiency at the design point of the test engine compared with the previous models.

In particular, in the Simple [39] model, which is an adiabatic model, several assumptions were made to simplify the complexity of the involved processes in the engine. This, in turn, resulted in predicting performance results that are much different to the actual engine performance results and yielding relative errors of over 100% (see, Table 3). On the other hand, the CAFS [48] and the Simple II [41] models (both adiabatic) did not consider the mass leakage through the displacer gap, which contributed significantly to the work loss in the engine, even though they discarded some of the assumptions made in the Simple model [39]. Further improvements were accomplished in the predicted energetic efficiency and the power output in the PSVL [42] and the PFST [36] models, by replacing the adiabatic with polytropic processes. Despite the improvements made using this approach, the failure of the authors to account for the leakage of the mass of the working fluid into the compression space has limited the accuracy of the models.

In the PSML [51], an updated model which was built on the principle of the polytropic processes in the cold and hot CVs and consequently, improved prediction errors of – 2.6% and + 3.78% in the brake power and energetic efficiency were recorded, respectively. This was achieved by considering the mass leakage into the compression space. Even so, the Present Model predicted the brake power from the engine more accurately than the PSML [51], because both the leakage into the compression space and the mass leakage into the crankcase have been simultaneously considered. Contrarily, the PSML [51] model predicted slightly better engine energetic efficiency compared to the Present Model. This is because the PSML model appreciates the polytropic losses of the engine, while the Present Model did not. Nevertheless, the reliance on experimental data to estimate the polytropic exponents in the compression and expansion processes of the engine using the PSML [51] model may limit its application and accuracy. Therefore, it can be concluded that the Present Model is evidently better than the previous models because of the improvements made in the traditional adiabatic model, by accounting for the mass leakage into the cold CV, mass leakage into the crankcase and shuttle heat loss in the engine. In addition, unlike in the previous models, modelling the instantaneous pressure of the working fluid in the CVs of the engine for each time step in the numerical process may have contributed to improving the accuracy of the Present Model.

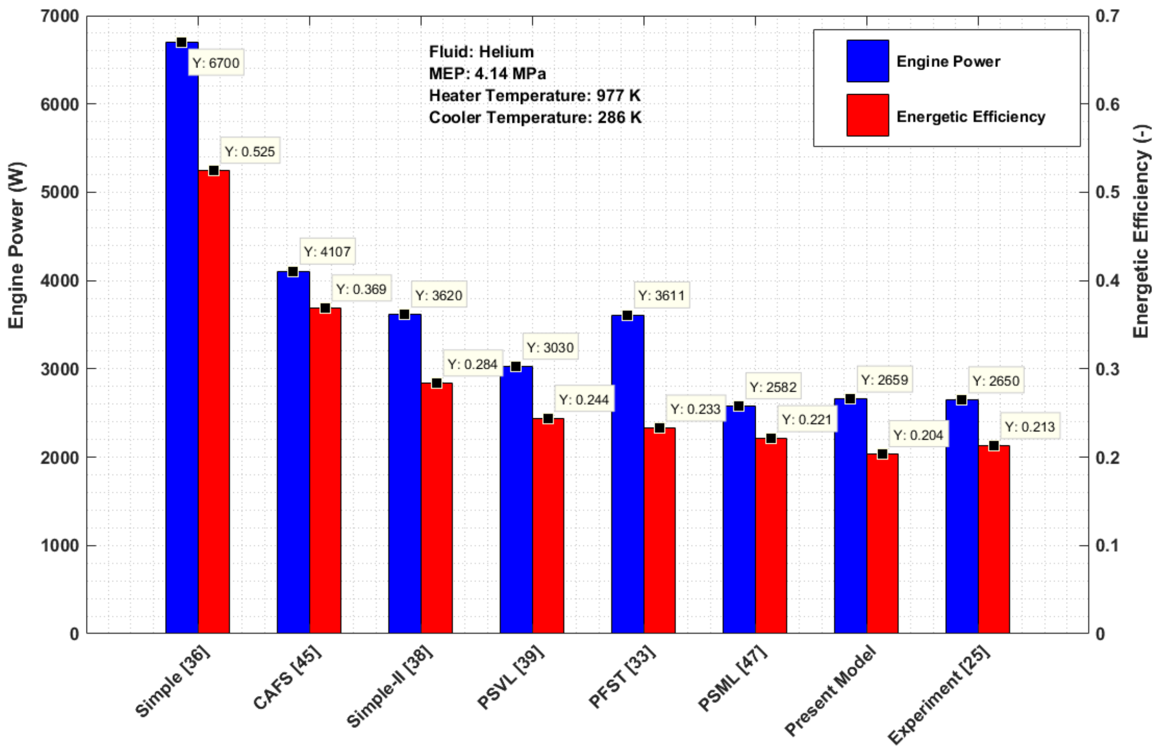

Fig. 4. Evaluating the prediction accuracy of the Present Model by comparing it with the experimental data and other numerical models' prediction.

Fig. 5 (a) and (b) evaluate the performance of the Present Model in predicting the experimental data (labelled 'Exp' in the legends) of the brake power of the GPU-3 engine at various frequencies to that of other theoretical models, when the engine is operating at a heater temperature of 922 K, cooler temperature of 286 K and for mean engine pressures of 4.14 MPa and 2.76 MPa, respectively. It is evident that the predicted brake power of the Present Model was very close to the experimental data at all the engine frequencies considered. In addition, a similar trend for the brake power is observed in the experimental results, the Present Model, the PFST [36] and the PSML [51], i.e., an initial increase with the increasing frequency of the engine before attaining a peak value at a frequency of 41.67 Hz. Subsequently, an appreciable decrease in the brake power was recorded as the frequency of the engine was increased beyond this value, especially when the engine is operating with a mean pressure of 4.14 MPa (Fig. 5 (a)).

This trend could be a result of the increase in the internal and the external irreversibilities in the engine due to the increase in the frequency of the rotation of the engine. Technically, at higher frequencies the flowrate of the gas in the engine would increase and consequently the ideal power will also increase, since the ideal work from the engine does not change. However, this increase in the flowrate of the gas could lead to an increase in the mechanical frictional

Table 3. Relative error in the prototype engine performance data predicted by the Present Model and other thermal models (T_{htr} = 977 K; T_k = 286 K; P_{mean} = 4.14 MPa; *Freq* = 41.67 Hz).

Source	**Simple** [39]	**CAFS** [48]	**Simple-II** [41]	**PSVL** [42]	**PFST** [36]	**PSML** [51]	**Present model This study**
Relative error in brake power (%)	**+ 152.8**	**+ 55.0**	**+ 36.6**	**+ 14.3**	**+ 36.3**	**- 2.6**	**+ 0.3**
Relative error in efficiency (%)	**+ 146.48**	**+ 73.24**	**+ 33.33**	**+ 14.55**	**+ 9.39**	**+ 3.78**	**- 4.02**

loss in the engine, FST loss, loss as a result of the pressure drop in the heat exchangers and even the spring hysteresis loss. The increased losses in the engine at high engine frequencies may offset the gain in the ideal power recorded, leading to a decline in the brake power derived from the engine.

It is evident from Fig. 5 (a) that when comparing the prediction accuracy of the Present Model to that of other models, the Present Model predicted the experimental engine's brake power more accurately for the entire engine frequencies investigated, compared with the Simple [39], Simple II [41], CAFS [48], PSVL [42], and PFST [36] models. On the other hand, compared with the PSML model, the Present Model predicted more superior results of the brake power of the GPU-3 engine for engine frequencies of 33 Hz – 54 Hz, while the PSML model predicted slightly better results for engine frequencies above 54 Hz. Similarly, based on Fig. 5 (b), the Present Model predicted superior results of the brake power for all engine frequencies investigated, compared with the Simple [39], Simple II [41], CAFS [48], PSVL [42], and PFST [36] models, except for frequencies above 53 Hz where the PFST [36] model predicted slightly better results than the Present Model. Conversely, except for frequencies between 16.67 Hz – 25 Hz where the predicted brake power between the Present Model and PSML model were comparable, the PSML model predicted the engine brake power more accurately than the Present Model for a mean effective pressure of 2.76 MPa.

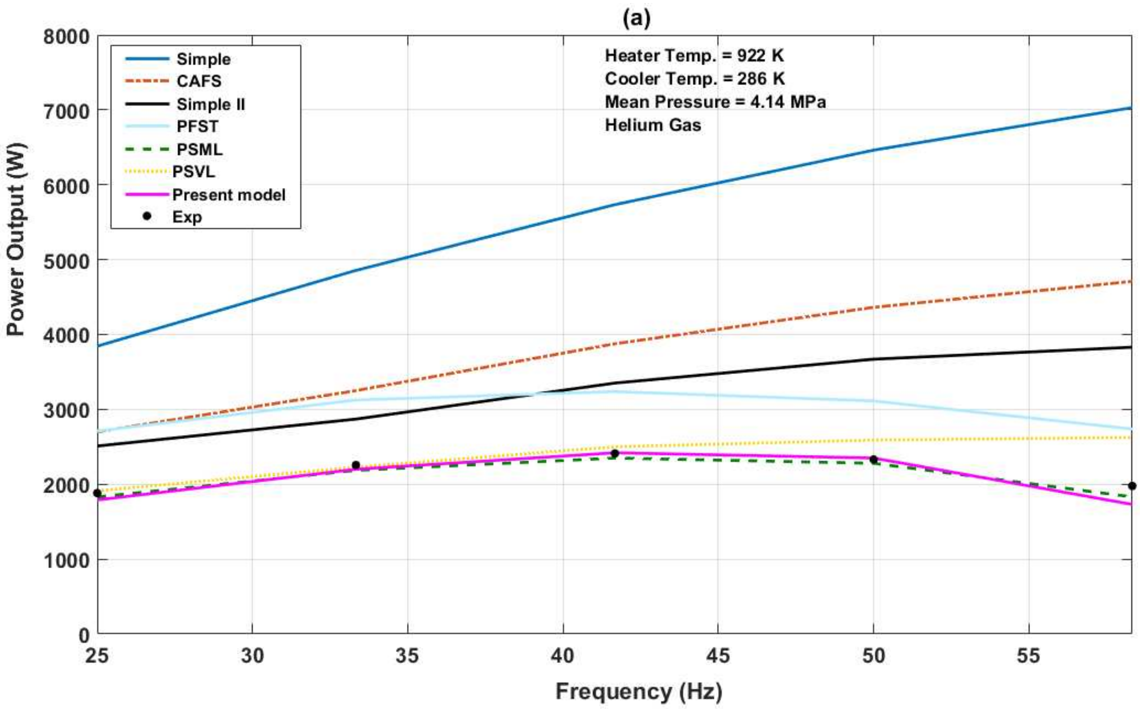

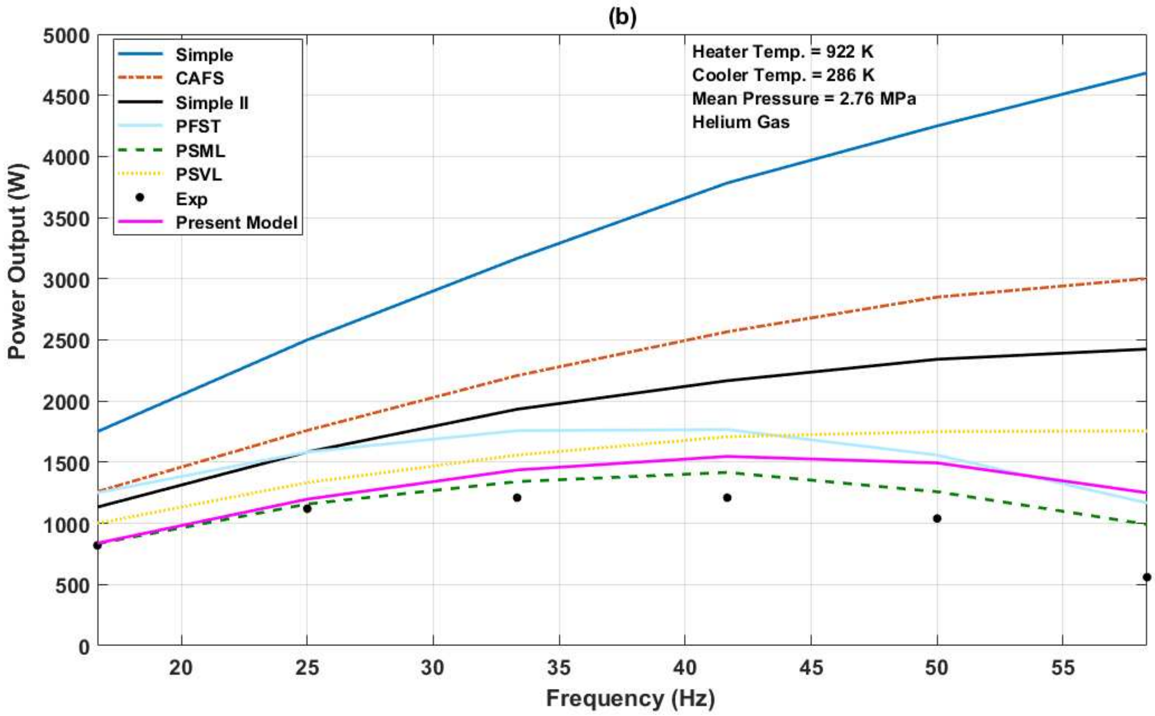

Fig. 5. Assessing the performance of the Present Model in estimating the brake power of the Prototype engine at various engine frequencies and comparing it to other thermal models (Simple [39], Simple II [41], CAFS [48], PSVL [42], PFST [36] , PSML [51]), and experimental data [28], at T_{htr} = 922 K, T_k = 286 K and *MEPs* of (a) 4.14 MPa, and (b) 2.76 MPa.

Fig. 6 (a) and (b) depict the relative error recorded in estimating the brake power of the prototype engine by the Present Model for *MEP* of 4.14 MPa and 2.76 MPa, respectively. It is seen that the prediction error was less than 15% (based on Fig. 6 (a)) and 40% (based on Fig. 6 (b)) for all the engine frequencies investigated, except for the unprecedented rise in the relative error at an engine frequency of 58.33 Hz for the second case. Meanwhile, compared with the Simple [39], Simple II [41], CAFS [48] and the PFST [36] models, the relative error recorded by the Present Model was significantly lower at all the engine frequencies investigated for the two *MEPs*, with the exemption of the PSVL [42] model where the relative error is comparable for engine frequencies between 25 Hz and 41.67 Hz for the *MEP* of 4.14 MPa. As for the more recent PSML [51] model, the Present Model recorded lower relative errors, for engine frequencies between 25 Hz and 41.67 Hz (as seen in Fig. 6 (a)), while the PSML [51] model produced lower relative errors at all the engine frequencies investigated except between 16.67 Hz and 25 Hz (as seen in the Fig. 6 (b)).

It can be concluded then that the Present Model can predict superior results for the brake power of the GPU-3 engine than all the existing second order thermal models at the design mean effective pressure of the engine (*MEP* = 4.14 MPa). However, the PSML [51] model predicted better results at the off-design condition (*MEP* of 2.76 MPa). This could be because in this study we considered the mass leakage into the crankcase. This requires the buffer pressure in the crankcase to be computed. Unfortunately, due to lack of information in the literature on the measured buffer pressure in the crankcase, we assumed the same buffer pressure for the design and off-design *MEP* cases; an assumption that may not be realistic in practice. High buffer pressures would imply lower pressure differentials between the compression space and the crankcase, leading to reduced leakage of gas into the crankcase [50]. Hence, the predicted brake work rate especially at high engine frequencies when the fluid is more mobile would be more than the actual power from the engine; similar to the trend observed in Fig. 6 (b).

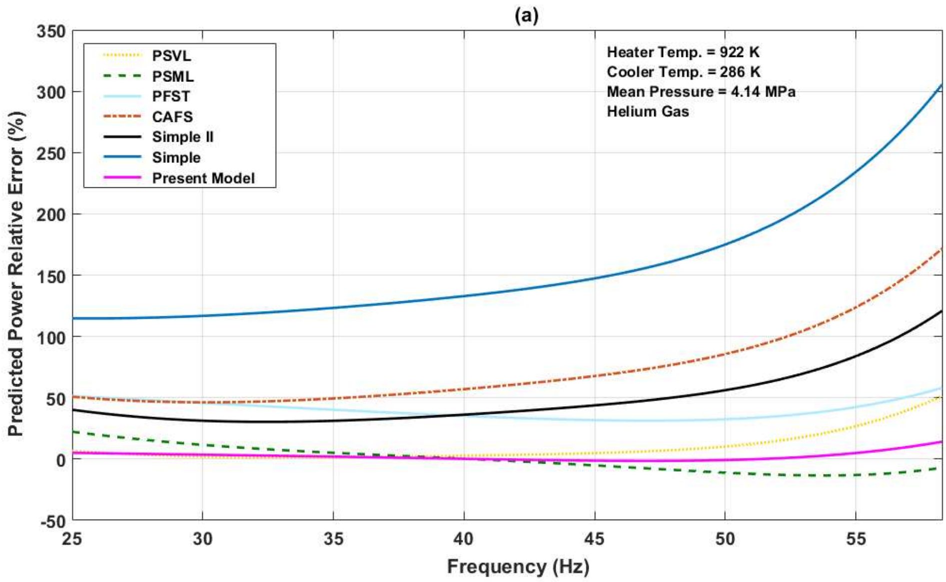

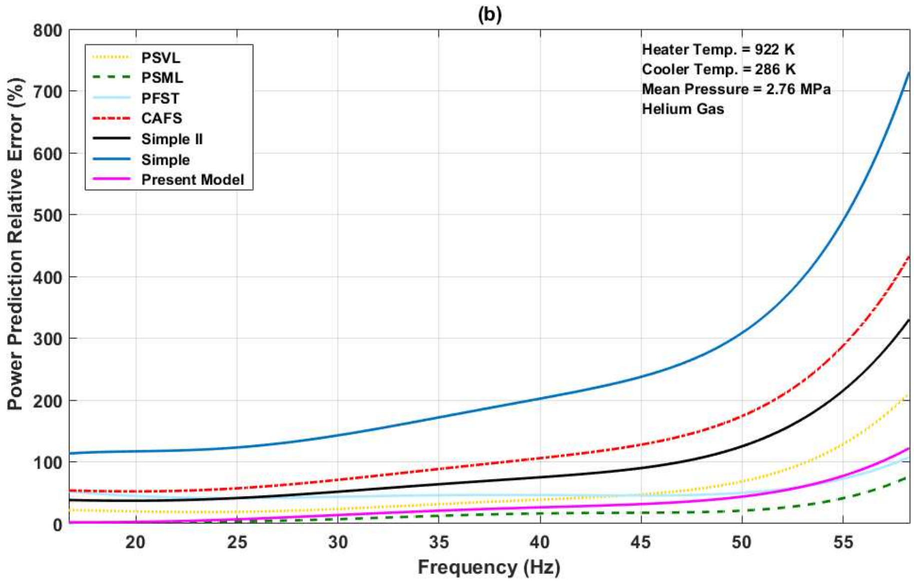

Fig. 6. Comparing the relative error in the predicted brake power of the Present Model at different engine frequencies with other models (Simple [39], Simple II [41], CAFS [48], PSVL [42], PFST [36], PSML [51]) at T_{htr} = 922 K, T_k = 286 K and *MEPs* of (a) 4.14 MPa, and (b) 2.76 MPa.

Fig. 7 (a) and (b) show the predicted energetic efficiency of the Present Model at various engine speeds compared with the predictions of other theoretical models, for the experimental engine operating at a heater temperature of 922 K, cooler temperature of 286 K and mean engine pressures of 4.14 MPa and 2.76 MPa, respectively. It is clear that the trend in the engine energetic efficiencies predicted by the Present Model is consistent with the experimental results for the full range of engine frequencies, and the mean effective pressures investigated. On the other hand, the other models predicted linear trends that do not coincide with the experimental dataset.

Meanwhile the predicted efficiencies of the Present Model are seen to have remained unchanged for engine frequencies between 25 Hz and 33.33 Hz for a *MEP* of 4.14 MPa or slightly increased for frequencies between 16.67 Hz and 25 Hz and remained the same until 33.33 Hz for a *MEP* of 2.76 MPa, before starting to decline appreciably in both cases. This is expected because the brake power output of the engine started to decline just after peaking at a frequency of 41.67 Hz. In addition, at higher engine frequencies the dissipation of the thermal energy in the regenerative engine becomes more intense, especially in the regenerator that contributes most of the losses in the engine. It has been mentioned in Section 2.2.2.1 that additional heat will be required to compensate for the imperfect regeneration, but at the cost of a decline in the energetic efficiency of the engine as is the case in Fig. 7 (a) and (b).

As seen from Fig. 7 (a), the energetic efficiencies predicted by the Present Model at *MEP* of 4.14 MPa were more accurate than the other models for all the engine frequencies investigated, except for the mid-range frequencies (33.33 Hz – 45 Hz) where the PSVL [42], and PFST [36], and PSML [51] models exhibit greater accuracy. Nevertheless, the consistency of the Present Model in estimating the engine’s energetic efficiency, makes it more superior compared to the other models. At *MEP* of 2.76 MPa (Fig. 7 (b)), the Present Model predicted superior results for engine frequencies ranging from 16.67 Hz to 41.67 Hz. However, between frequency of 41.67 Hz and 58.33 Hz, the PSML and PFST feature higher accuracy.

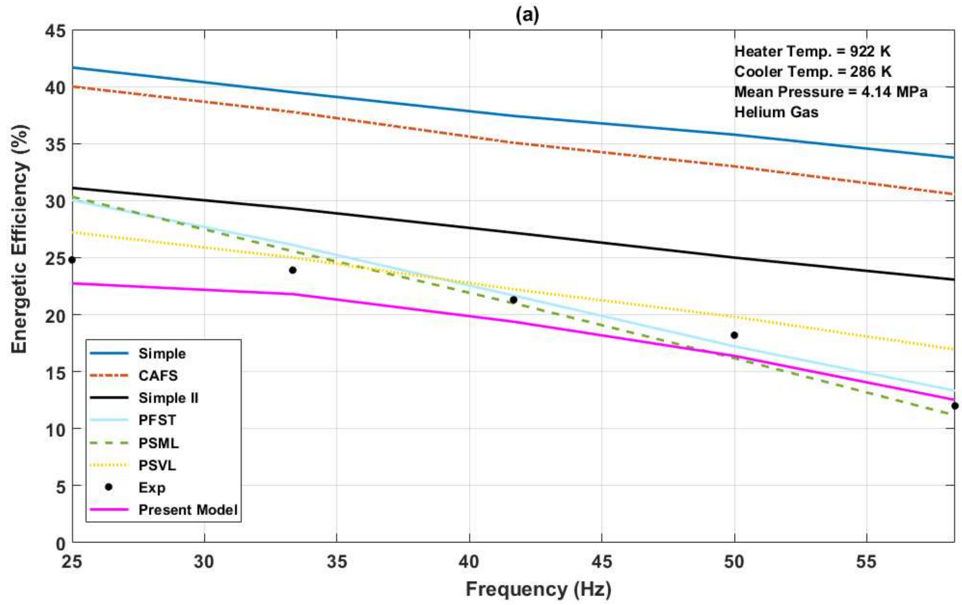

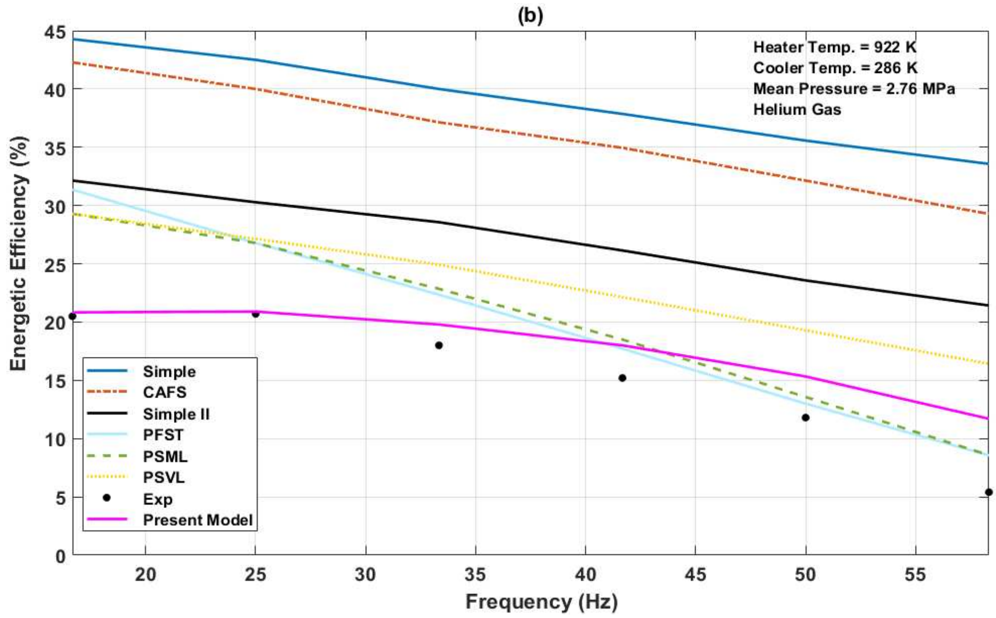

Fig. 7. Assessing the precision of the Present Model in estimating the energetic efficiency of the prototype Stirling engine at different engine frequencies and comparing it to previous models (Simple [39], Simple II [41], CAFS [48], PSVL [42], PFST [36], PSML [51]) and experimental data [28], at T_{htr} = 922 K, T_k = 286 K and *MEPs* of (a) 4.14 MPa, and (b) 2.76 MPa.

Fig. 8 (a) and (b) show the relative error recorded in estimating the energetic efficiency of the prototype Stirling engine by the Present Model for *MEP* of 4.14 MPa and 2.76 MPa, respectively. It is seen that an average prediction error of -10% (based on Fig. 8 (a)) and 25% (based on Fig. 8 (b)) were obtained for all the engine frequencies investigated. The Present model produce lower prediction errors than all previous models for the entire range of frequencies with the exemption of the PSVL [42], PFST [36] and the PSML [51], that yield lower relative errors at the mid-range frequencies and at the design *MEP* of 4.14 MPa. While for the off-design *MEP* of 2.76 MPa (Fig. 8 (b)) only the PFST [36] and the PSML [51] predicted the energetic efficiency of the engine with lower relative errors, for engine frequencies above 41.67 Hz. This observed trend further validates our initial position that the Present Model is more superior to the previous models in predicting the performance of the engine at the design *MEP* of 4.14 MPa.

Finally, the relative consistency of the enhanced model developed in this paper in predicting the brake power and energetic efficiency of the GPU-3 Stirling engine, at low, medium and high engine frequencies, especially at the design point of the engine, makes it suitable and superior to previous thermal models for deployment in studies involving dynamic operation of the engine.

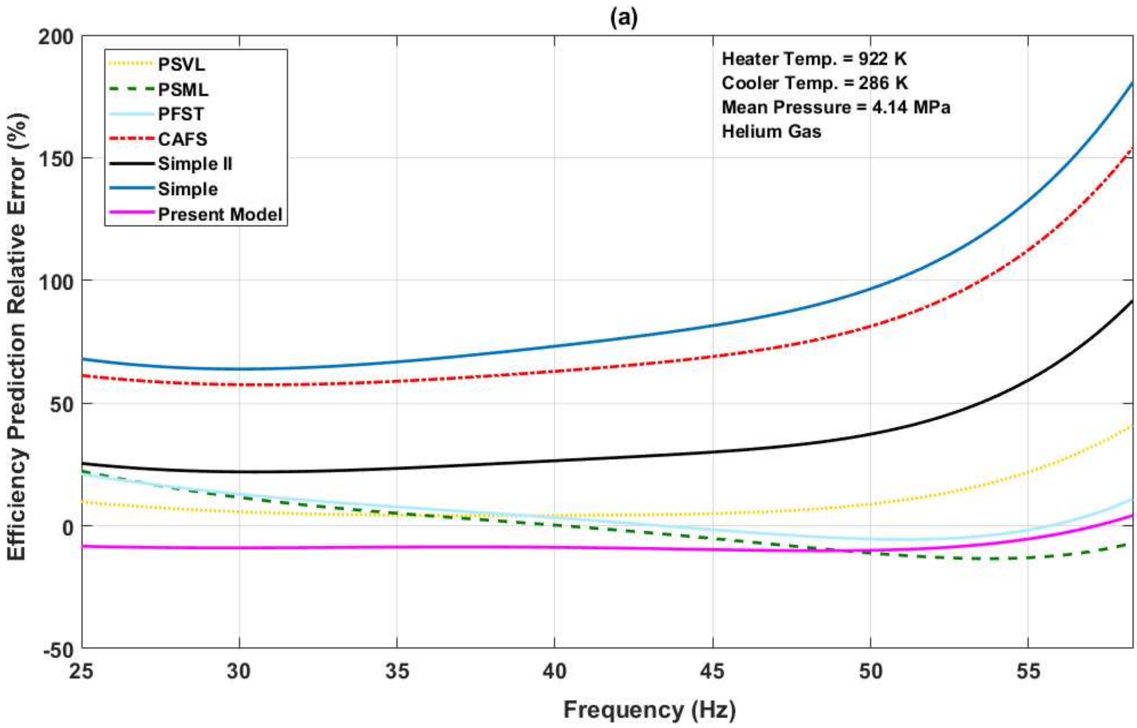

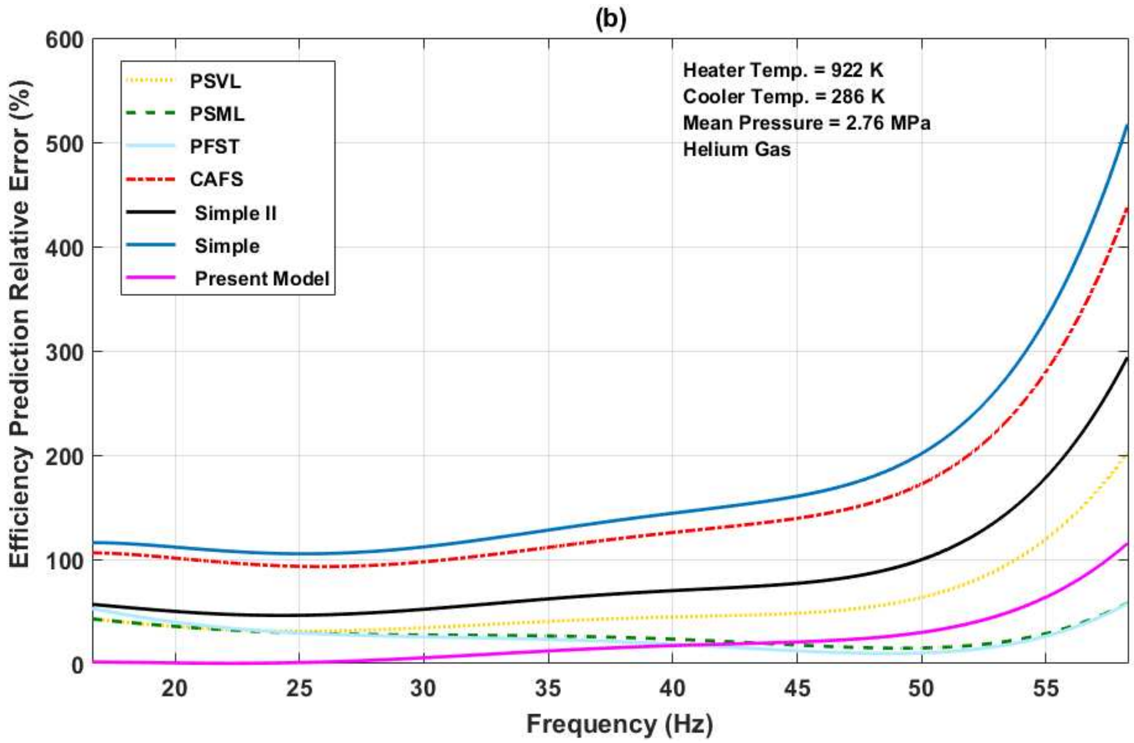

Fig. 8. Comparing the relative error incurred by the Present Model in estimating the energetic efficiency of the prototype Stirling engine at different engine operating frequencies, with previous models (Simple [39], Simple II [41], CAFS [48], PSVL [42], PFST [36], PSML [51]) at T_{htr} = 922 K, T_k = 286 K and *MEPs* of (a) 4.14 MPa, and (b) 2.76 MPa.

5. Performance Simulation of the GPU-3 engine using the Present Model

In this section, we present the impact of the key engine geometrical and physical properties on the performance of the GPU-3 engine. These properties are the dimensionless gap number, the heater temperature and the cooler temperature. The performance of the engine using helium and hydrogen as working fluid has been tested and compared for three distinct engine frequencies and mean effective pressures.

Fig. 9, 10 and 11 show the impact of the dimensionless gap number (J/D_{d}) – the ratio of the clearance between the displacer and engine cylinder to the displacer diameter – on the brake power of the prototype Stirling engine operating with a heater wall temperature of 977 K, cooler wall temperature of 286 K, engine frequencies of 25 Hz, 33.33 Hz and 41.67 Hz and mean effective pressures (MEP) of 4.14 MPa, 2.76 MPa and 1.38 MPa, respectively. In Fig. 9, it is observed that for the two engine gases (helium and hydrogen) and for all the engine frequencies investigated, the brake power of the engine did not change remarkably, when the dimensionless gap number was below 1.5×10^{-4}. However, as the dimensionless gap number increases, the brake power declines drastically. This is because with the increase in the gap between the displacer and the wall of the cylinder, more of the internal gas in the engine will leak from the hot CV into the cold CV. Thus, there will be loss in the expansion work of the engine, leading to a corresponding gain in the compression work; hence, the net ideal work from the engine will decline. In addition, it is seen that the impact of the dimensionless gap number on the brake power is less intense at an engine frequency of 25 Hz, but becomes significant as the frequency increases from 33.3 Hz to 41.67 Hz. Consequently, the design point of the engine, $J/D_{\mathrm{d}} = 4.0 \times 10^{-4}$, drifted further from the optimum brake power with an increase in the operating frequency.

Comparing the two working fluids, the impact of the dimensionless gap number on the brake power output of the engine is more severe for the engine utilizing hydrogen gas at all the frequencies investigated. This is because hydrogen is lighter and this results to increased leakage into the compression space. Thus, the engine working with helium has its design point closer to the optimum power output than that operating on hydrogen gas.

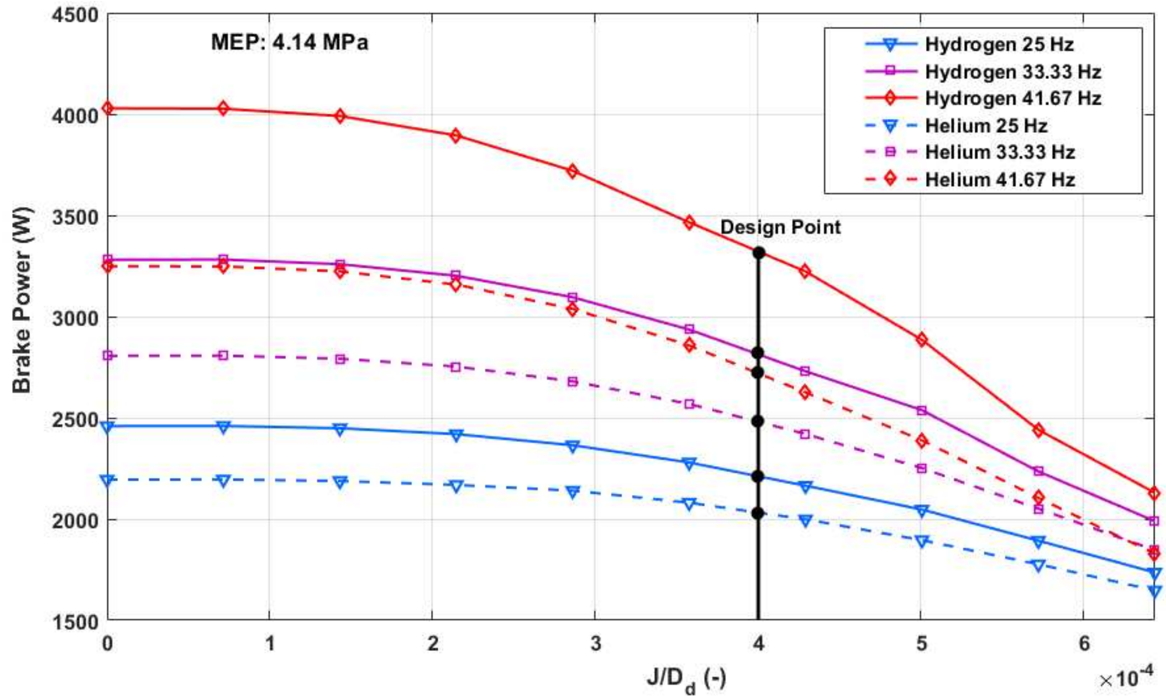

Fig. 9. Comparing the impact of the gap dimensionless number on the brake-power of the prototype Stirling engine, operating at different engine frequencies, $T_{\mathrm{htr}} = 977$ K, $T_{\mathrm{k}} = 286$ K, *MEP* of 4.14 MPa and utilizing helium or hydrogen as the working fluid.

Similarly, from Fig. 10, the change in the brake power of the engine became noticeable when the dimensionless gap number exceeded 2.0×10^{-4}, for *MEP* of 2.76 MPa. As in the case of the engine operating with *MEP* of 4.14 MPa, the brake power of the engine deteriorated significantly with the increase in the dimensionless gap number beyond this value. Nevertheless, the impact is less intense for helium gas than for hydrogen gas. Meanwhile, as the frequency of the engine increased the impact increased, while the design point of the engine was increasingly sub-optimal. However, compared with the engine operating at *MEP* of 4.14 MPa, the deterioration of the brake power with the increase in the dimensionless gap number was less severe at *MEP* of 2.76 MPa.

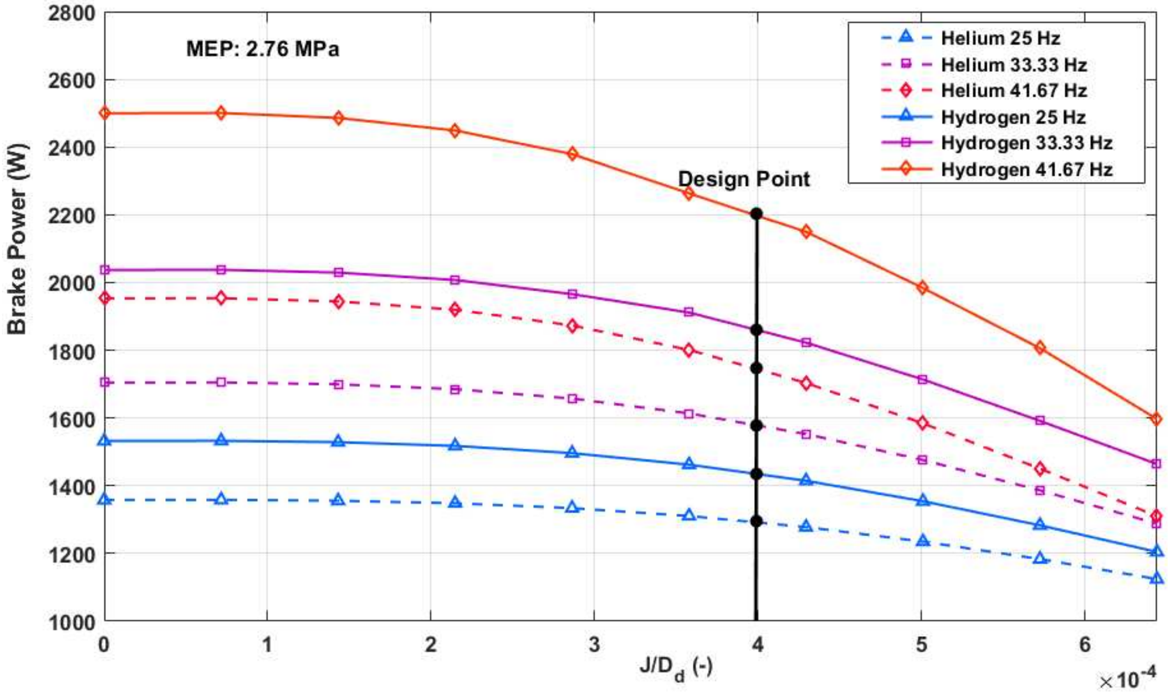

Fig. 10. Comparing the impact of the gap dimensionless number on the brake-power of the prototype Stirling engine operating at different engine frequencies, T_{htr} = 977 K, T_k = 286 K and *MEP* of 2.76 MPa and utilizing helium or hydrogen as the working fluid.

Likewise, based on Fig. 11, appreciable changes in the brake power output from the GPU-3 engine did not occur until a dimensionless gap number of 3.0×10^{-4} was attained for the engine operating with a *MEP* of 1.38 MPa. Beyond this value, the brake power reduced significantly with the increase in the dimensionless gap number; however, the impact was not as pronounced as in the case of *MEPs* of 2.76 MPa and 4.14 MPa. Meanwhile, comparing the two working fluids, the impact of the dimensionless gap number on the brake power is again more significant for hydrogen than for helium, while the change in the engine frequency had a similar impact as in the case of the engine operating with *MEPs* of 2.76 MPa or 4.14 MPa. However, the design point of the prototype engine is almost at the optimal brake-power in this case than in the previous cases. Hence, the increase in the *MEP* of the engine contributed to the negative impact of the dimensionless gap number on the brake power of the GPU-3 engine. Similarly, an increase in the frequency of the engine, led to an increase in the deterioration of the power output as the dimensionless gap number increased with the effect being more pronounced in the engine utilizing hydrogen [43,65]. Finally, at the design point of the GPU-3

Stirling engine, reducing the dimensionless gap number from 4.0×10^{-4} to 2.0×10^{-4} would lead to 16% increase in the brake power from the engine if helium gas is used as the working fluid and 15% with hydrogen gas.

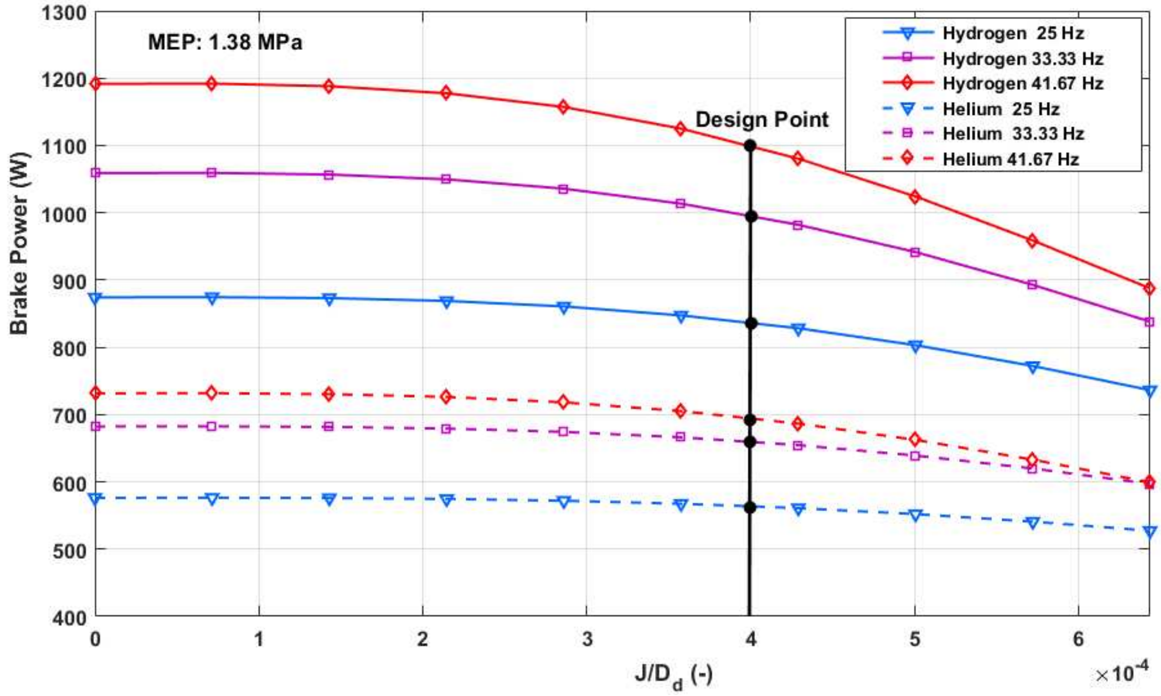

Fig. 11. Comparing the impact of the gap dimensionless number on the prototype Stirling engine, operating at different engine frequencies, T_{htr} = 977 K, T_k = 286 K and *MEP* of 1.38 MPa and utilizing helium or hydrogen as the working fluid.

Fig. 12, 13 and 14 show the impact of the dimensionless gap number on the energetic efficiency of the GPU-3 engine using helium or hydrogen and operating at a heater temperature of 977 K, cooler temperature of 286 K engine frequencies of 25 Hz, 33.33 Hz, and 41.67 Hz and mean effective pressures (MEP) of 4.14 MPa, 2.76 MPa and 1.38 MPa, respectively. It is clear from Fig. 12 that for both engine gases, the energetic efficiency of the engine started deteriorating significantly when the dimensionless gap number increased beyond 1.5×10^{-4}. As described in eq.(2), with an increase in the displacer gap the shuttle thermal loss decreases, thus resulting in a decrease in the energetic efficiency of the engine [51]. The decrease in the energetic efficiency is, however, more pronounced with hydrogen than with helium, since the brake power deteriorated more in the former. Meanwhile, the energetic efficiencies were higher at higher frequencies for smaller dimensionless gap number, but become lower when this number increases. This is because the work losses in the engine deteriorated with the increase in the frequency of the engine and the dimensionless gap number. Again, the engine working with helium gas has energetic efficiency at the design point closer to the optimum energetic efficiency compared with the hydrogen engine.

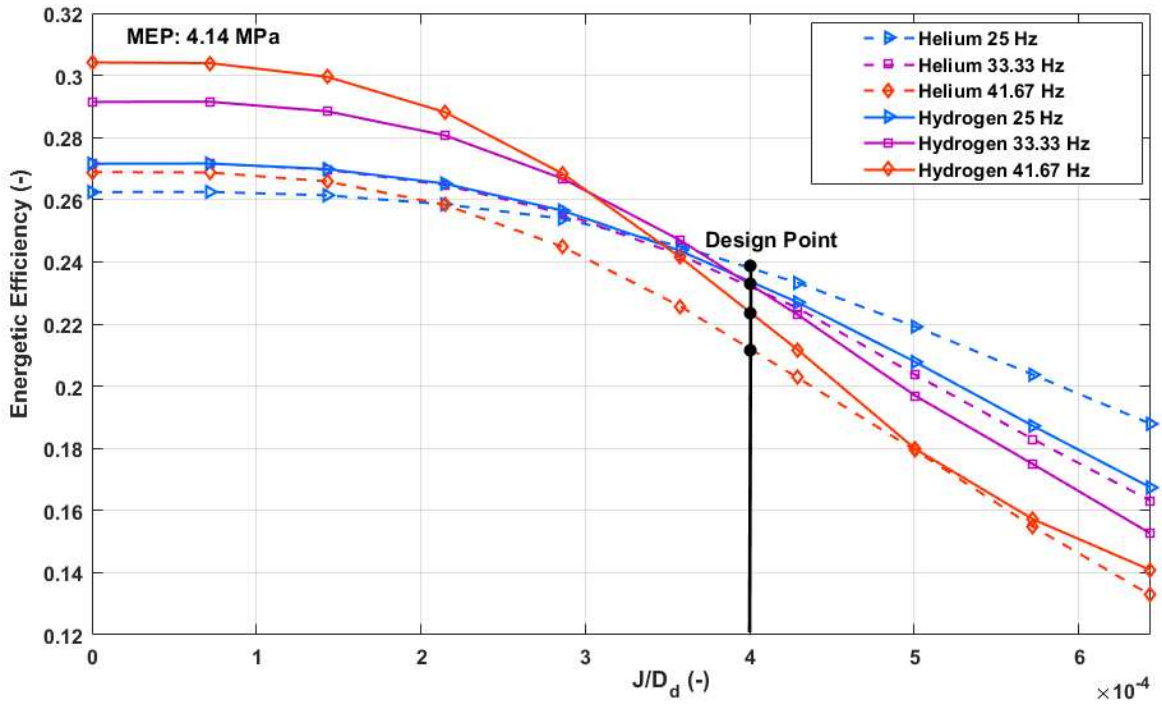

Fig. 12. Comparing the impact of the dimensionless gap number on the thermal efficiency of the prototype Stirling engine, for different engine frequencies, T_{htr} = 977 K, T_k = 286 K and *MEP* of 4.14 MPa and utilising helium gas or hydrogen as the working fluid.

A similar trend as in the case of the engine working with *MEP* of 4.14 MPa can be seen in Fig. 13, except that appreciable changes in the energetic efficiency of the engine were only observed after a dimensionless gap number of 2.0×10^{-4}. This is expected, since the brake power produced from the engine remained the same for dimensionless gap number below this value. However, the change in the energetic efficiency observed for *MEP* of 2.76 MPa was less severe compared with the case of *MEP* of 4.14 MPa. While the energetic efficiency of the engine at the design point was much closer to the optimal engine efficiency, especially with the decrease in the frequency of the engine.

The impact of the dimensionless gap number on the energetic efficiency of the GPU-3 engine was not so significant at *MEP* of 1.38 MPa, as seen in Fig. 14, especially for the engine using helium. It is rather seen that, at this low *MEP*, the frequency of the helium engine had more impact on the energetic efficiency than the dimensionless gap number. For the engine running on hydrogen, the dimensionless gap number still maintained similar impact on the engine for *MEP* of 1.38 MPa as in the other cases, although the impact is less intense in this case. Finally, the energetic efficiency of the GPU-3 Stirling engine could improve by 22% for helium and 30% for hydrogen, if the dimensionless gap number is reduced from 4.0×10^{-4} to 2.0×10^{-4}.

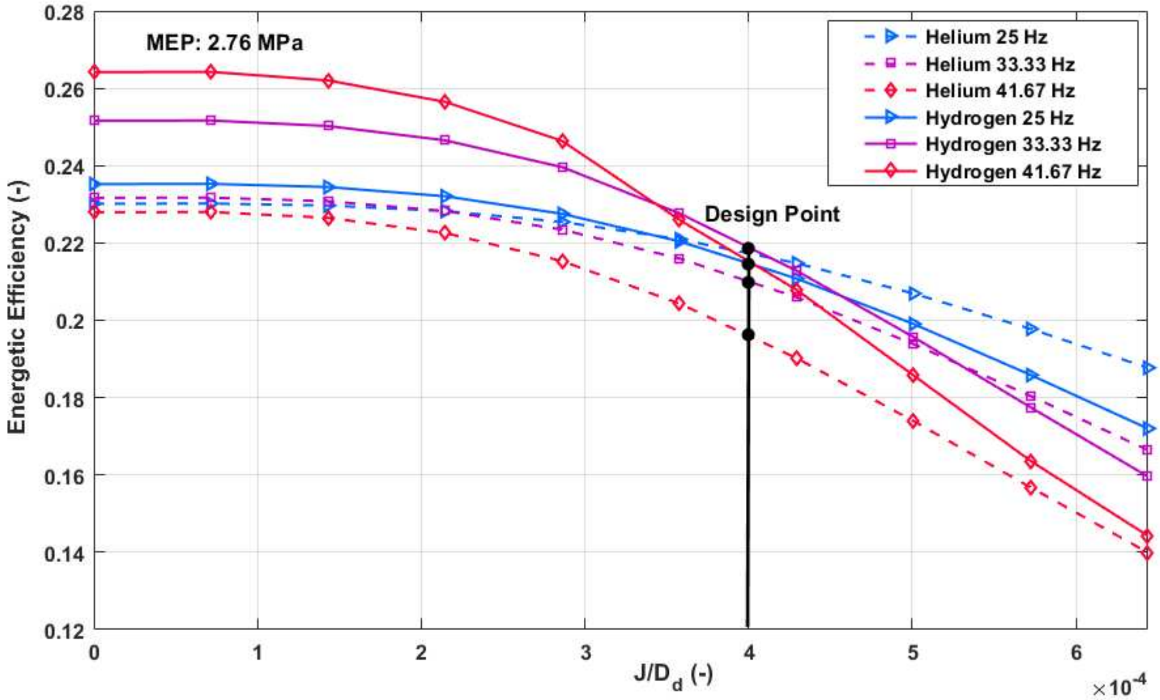

Fig. 13. Comparing the impact of the dimensionless gap number on the energetic efficiency of the prototype Stirling engine, for different engine frequencies, T_{htr} = 977 K, T_k = 286 K and *MEP* of 2.76 MPa and utilising helium gas or hydrogen as the working fluid.

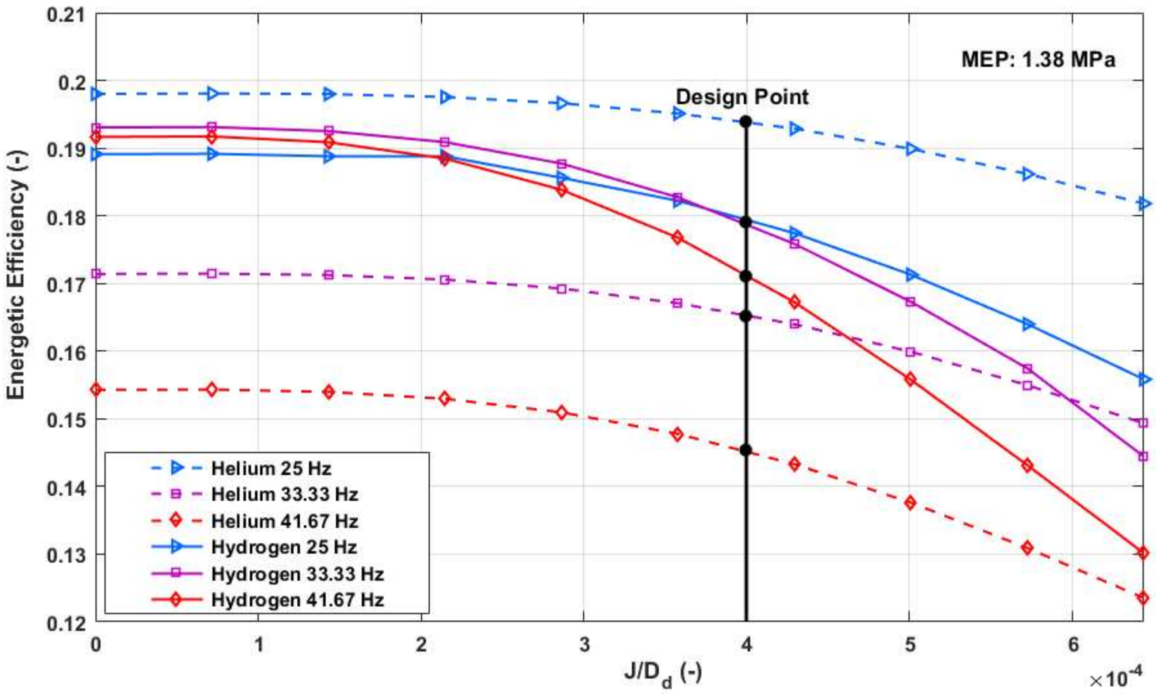

Fig. 14. Comparing the impact of the dimensionless gap number on the energetic efficiency of the prototype Stirling engine, for different engine frequencies, T_{htr} = 977 K, T_k = 286 K and *MEP* of 1.38 MPa and utilising helium gas or hydrogen as the working fluid.

Fig. 15 shows the impact of the increase in the heater temperature on the brake work rate of the GPU-3 engine operating with a frequency of 41.67 Hz, cooler temperature of 286 K, mean effective pressures of 4.14 MPa, 2.76 MPa and 1.38 MPa, respectively, and using hydrogen or helium as its working fluid. As is clear, the heater temperature impacts on the brake power positively for all the *MEPs* of the engine investigated, and using either hydrogen or helium. However, it is seen that the amplitude of the increase in the brake power reduces significantly at higher temperatures. Similarly, the increase in the *MEP* of the engine results in a significant increase in the brake power. For an increase in the heater temperature from 450 ℃ to 850 ℃, the brake power trebled when helium gas was used as the working fluid of the engine, while the value doubled with hydrogen gas, for all the *MEPs* of the engine considered. It is possible to improve the brake power by 18%, by increasing the temperature of the heater from the design temperature of 703 ℃ to 850 ℃ when using helium, or by 10% with hydrogen.

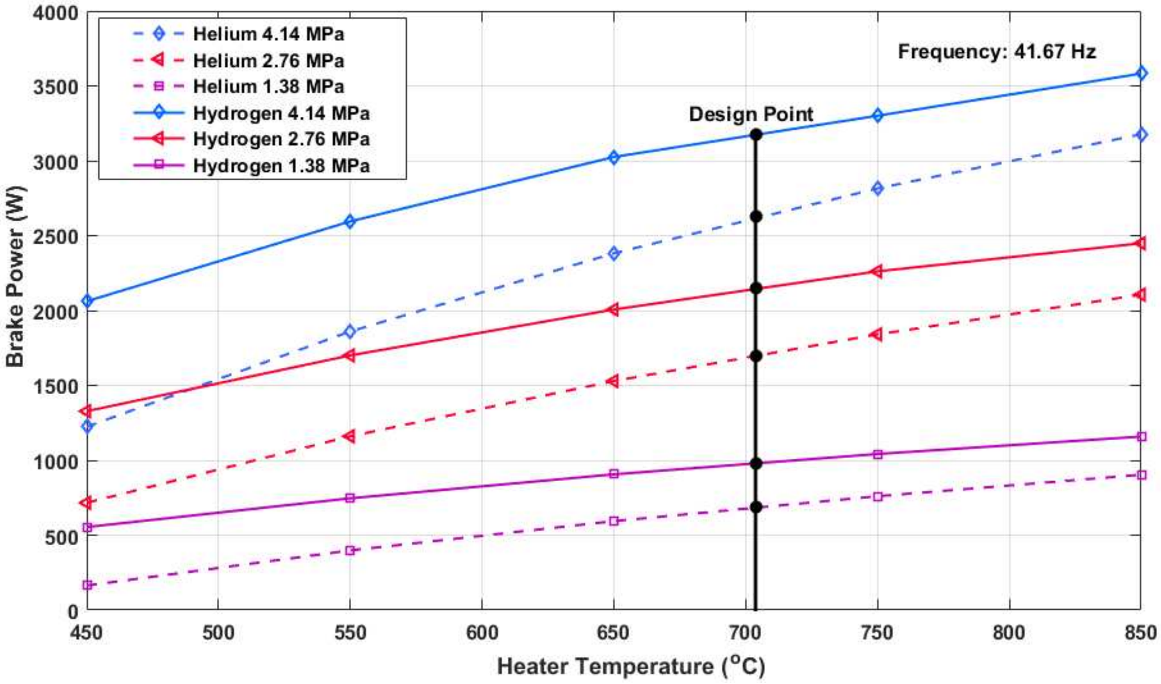

Fig. 15. Comparing the impact of the heater temperature on the brake power of the prototype Stirling engine, for T_k = 286 K, frequency of 41.67 Hz and for different *MEPs*, using helium gas and hydrogen as the working fluid.

Fig. 16 presents the impact of increasing the heater temperature on the energetic efficiency of the Stirling engine, for different *MEPs*, while keeping the operating frequency of the engine constant and equal to 41.67 Hz. It can be observed that as the temperature of the heater increases, the energetic efficiency of the engine increases remarkably, especially for the case when helium has been deployed as the working fluid of the engine. However, the trend slowed down significantly at very high heater temperatures. In particular, in the case of the hydrogen engine, the energetic efficiency did not increase substantially beyond a heater temperature of 750 ℃ (for *MEP* of 2.76 MPa and 4.14 MPa). Meanwhile, it is seen that an appreciable increase in the energetic efficiency cannot be achieved with the increase in the *MEP* of the engine beyond 4.14 MPa for hydrogen [28,41]. Finally, a 10% increase in the energetic efficiency of the helium engine can be achieved at the design *MEP* of 4.14 MPa, if the temperature of the heater increases from 703 ℃ to 850 ℃ .

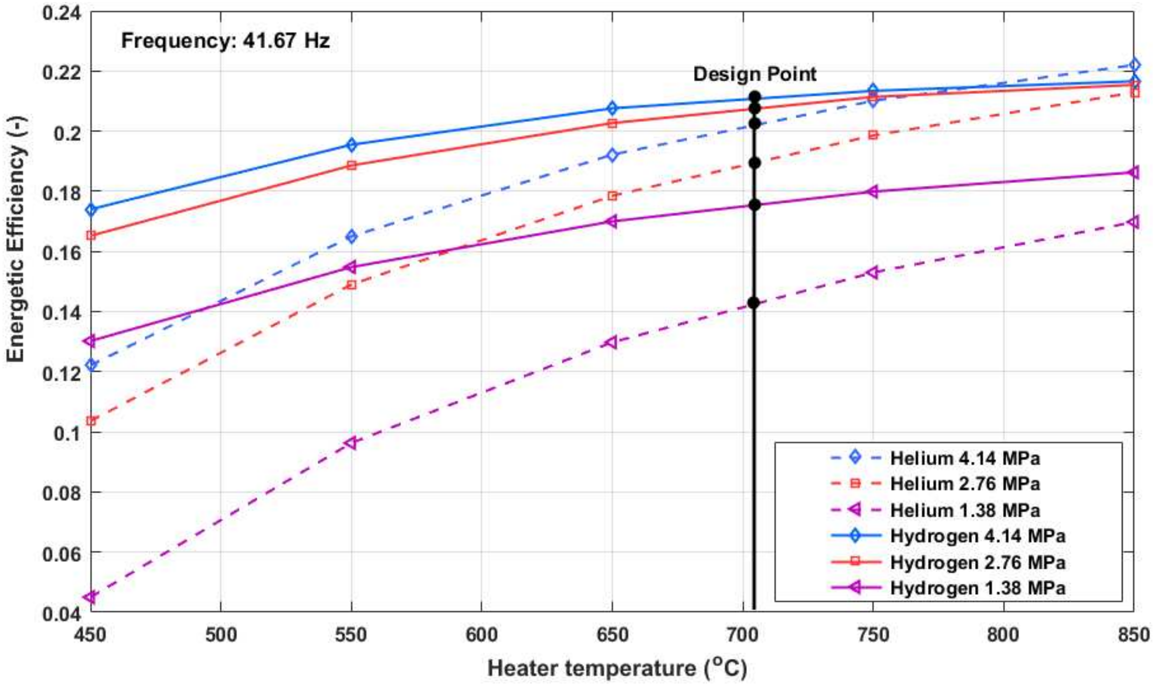

Fig. 16. Comparing the impact of the heater temperature on the energetic efficiency of the prototype Stirling engine, for T_k = 286 K, frequency of 41.67 Hz and for different *MEPs*, using helium gas and hydrogen as the working fluid.

Fig. 17 (a) and (b) present the simultaneous impact of the heater and cooler temperature on the brake power and energetic efficiency of the GPU-3 engine operating at a frequency of 50 Hz, *MEP* of 4.14 MPa and utilising helium or hydrogen as its working fluid. As seen in Fig. 17 (a) and (b), the simultaneous increase of the heater temperature and decrease of the cooler temperature results in an increase in the brake power and energetic efficiency, respectively. The increase is more significant for the helium engine compared with the hydrogen engine. Specifically, an increase in the heater temperature from the design point of 703 ℃ to 850 ℃, and a corresponding decrease in the cooler temperature from 13 ℃ to 0 ℃ results in a 32% and 18% increase in the brake power and energetic efficiency of the helium engine, respectively.

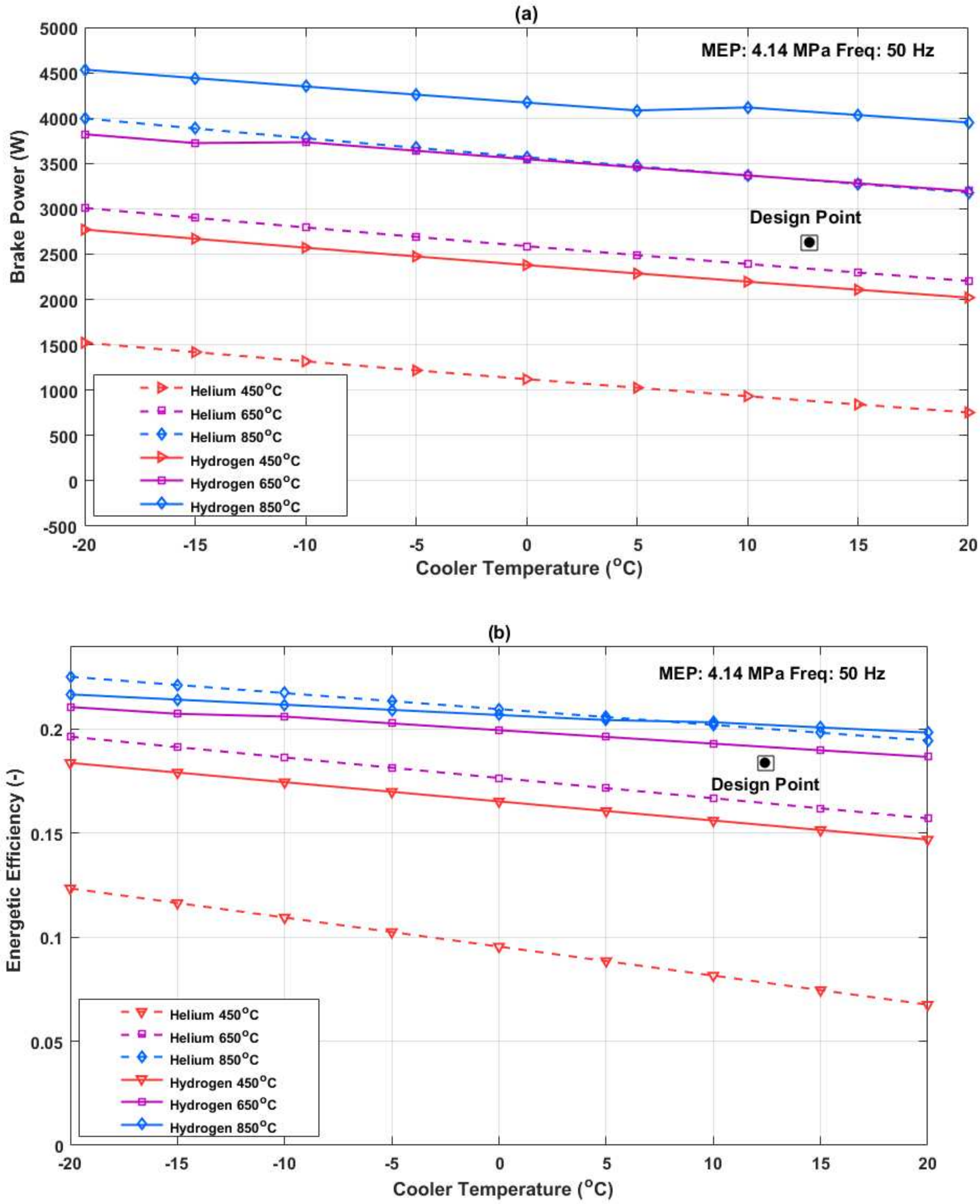

Fig. 17. Comparing the impact of the heater and cooler temperatures on the (a) brake power, and (b) energetic efficiency of the prototype Stirling engine, for *MEP* of 4.14 MPa and frequency of 50 Hz using helium gas and hydrogen as the working fluid.

6. Conclusion

A new thermal model has been developed in this paper, based on the modifications of the traditional adiabatic model of the Stirling engine. Therefore, for the first time the mass leakage from the expansion volume into the compression volume, the mass leakage from the working volume into the crankcase and the displacer shuttle loss were coupled into the governing differential equations of the simple adiabatic models of the Stirling engine. Similar to previous thermal models, second and third category losses such as, piston finite speed loss, mechanical friction loss, spring hysteresis loss, regenerator imperfection loss, heat conduction loss, enthalpy leakage loss and dissipation loss were also considered in developing the present thermal model. Conversely, in the Present Model, the instantaneous pressure in the control volumes of the engine were determined with the computed hydraulic losses in the engine, and the value used to update the temperatures in the control volumes for each time step.

The developed model was evaluated with the data of the General Motors GPU-3 engine. It was found that the modifications made in the traditional model in this paper, substantially improved the prediction accuracy of the present model, thus making it superior to previous thermal models. It was found that the brake power of the experimental engine was estimated with greater accuracy using the Present Model compared with all the previous numerical and closed-form models at all the engine frequencies investigated, apart from the newly developed PSML [51] model that predicted better results at higher engine frequencies. Whilst the predicted energetic efficiency was more consistent with the experimental data, at all the engine frequencies investigated, contrary to other models that predicted linear trends. It was finally concluded that the new model developed in this paper would be more suitable for deployment in studies involving the dynamic operation of the Stirling engine, since it is consistent in predicting accurate experimental data at all engine speeds.

The impact of the dimensionless gap number on the brake power and energetic efficiency of the experimental engine at different mean effective pressures and engine operating frequencies was also assessed, and compared for hydrogen and helium working fluids. It was found that for a given mean effective pressure, a minimum dimensionless gap number exists below which the performance of the engine becomes insensitive to the displacer gap. This minimum dimensionless gap number decreases with increasing the mean effective pressure in the engine, but varied slightly with the working fluid and the frequency of the engine. Furthermore, it was also found that the design point dimensionless gap number for different mean effective pressure and frequency of the engine is slightly higher than the corresponding minimum dimensionless gap number which depends on the type of the working fluid. Hence, it was concluded that the brake power and energetic efficiency of the engine could be improved significantly by optimizing the design of the cylinder wall-displacer gap, especially if hydrogen serves as the working fluid of the engine.

Also, the variation of the brake power and energetic efficiency with the heater and cooler temperature was examined. It was found that whilst the heater temperature had a positive impact on the brake work rate and energetic efficiency of the GPU-3 engine, the cooler temperature produced the opposite effect. This effect was more pronounced in the engine working with helium than hydrogen, and the amplitude decreased with the increase in the mean effective pressure of the engine. An optimum mean effective pressure is required for optimum efficiency of the engine, which depends strongly on the selection of the working fluid. Based on the comparative performance analysis, it was found that the optimum mean effective pressure is closer to the design point of the GPU-3 engine for the hydrogen case compared to the helium case. Thus, at the design mean effective pressure of the prototype engine, lowering the cooler temperature (e.g. using cold exergy stored in cryogenic fluids [13]), and increasing the heater temperature, as much as it is practically feasible could be a plausible way to improve on the performance of the engine for any of the working fluids.

Acknowledgements

This study was funded by the Petroleum Technology Development Fund, an agency of the Ministry of Petroleum Resources, in Nigeria.

References

[1] Rajbongshi R, Borgohain D, Mahapatra S. Optimization of PV-biomass-diesel and grid base hybrid energy systems for rural electrification by using HOMER. Energy 2017;126:461–74. doi:10.1016/j.energy.2017.03.056.

[2] Kaabeche A, Ibtiouen R. Techno-economic optimization of hybrid photovoltaic/wind/diesel/battery generation in a stand-alone power system. Sol Energy 2014;103:171–82. doi:10.1016/j.solener.2014.02.017.

[3] Shezan SA, Julai S, Kibria MA, Ullah KR, Saidur R, Chong WT, et al. Performance analysis of an off-grid wind-PV (photovoltaic)-diesel-battery hybrid energy system feasible for remote areas. J Clean Prod 2016;125:121–32. doi:10.1016/j.jclepro.2016.03.014.

[4] Wang E, Yu Z, Zhang H, Yang F. A regenerative supercritical-subcritical dual-loop organic Rankine cycle system for energy recovery from the waste heat of internal combustion engines. Appl Energy 2017;190:574–90. doi:10.1016/j.apenergy.2016.12.122.

[5] González A, Riba JR, Puig R, Navarro P. Review of micro- and small-scale technologies to produce electricity and heat from Mediterranean forests' wood chips. Renew Sustain Energy Rev 2015;43:143–55. doi:10.1016/j.rser.2014.11.013.

[6] Ferreira AC, Nunes ML. IMECE2014-38529 Numerical study of regenerator

configuration in the design of a stirling 2018:1–10.

[7] Kimming M, Sundberg C, Nordberg Å, Baky A, Bernesson S, Norén O, et al. Biomass from agriculture in small-scale combined heat and power plants - A comparative life cycle assessment. Biomass and Bioenergy 2011;35:1572–81. doi:10.1016/j.biombioe.2010.12.027.

[8] Hooshang M, Askari Moghadam R, AlizadehNia S. Dynamic response simulation and experiment for gamma-type Stirling engine. Renew Energy 2016;86:192–205. doi:10.1016/j.renene.2015.08.018.

[9] Thombare DG, Verma SK. Technological development in the Stirling cycle engines. Renew Sustain Energy Rev 2008;12:1–38. doi:10.1016/j.rser.2006.07.001.

[10] Sowale A, Kolios AJ, Fidalgo B, Somorin T, Parker A, Williams L, et al. Thermodynamic analysis of a gamma type Stirling engine in an energy recovery system. Energy Convers Manag 2018;165:528–40. doi:10.1016/j.enconman.2018.03.085.

[11] Maraver D, Sin A, Royo J, Sebastián F. Assessment of CCHP systems based on biomass combustion for small-scale applications through a review of the technology and analysis of energy efficiency parameters. Appl Energy 2013;102:1303–13. doi:10.1016/j.apenergy.2012.07.012.

[12] Kuhn V, Klemeš J, Bulatov I. MicroCHP: Overview of selected technologies, products and field test results. Appl Therm Eng 2008;28:2039–48. doi:10.1016/j.applthermaleng.2008.02.003.

[13] Alfarawi S, Al-Dadah R, Mahmoud S. Enhanced thermodynamic modelling of a gamma-type Stirling engine. Appl Therm Eng 2016;106:1380–90. doi:10.1016/j.applthermaleng.2016.06.145.

[14] Alfarawi S, AL-Dadah R, Mahmoud S. Potentiality of new miniature-channels Stirling regenerator. Energy Convers Manag 2017. doi:10.1016/j.enconman.2016.12.017.

[15] Najafi Amel A, Kouravand S, Zarafshan P, Kermani AM, Khashehchi M. Study the Heat Recovery Performance of Micro and Nano Metfoam Regenerators in Alpha Type Stirling Engine Conditions. Nanoscale Microscale Thermophys Eng 2018;22:137–51. doi:10.1080/15567265.2018.1456581.

[16] Ipci D, Karabulut H. Thermodynamic and dynamic analysis of an alpha type Stirling engine and numerical treatment. Energy Convers Manag 2018;169:34–44. doi:10.1016/j.enconman.2018.05.044.

[17] Araoz JA, Salomon M, Alejo L, Fransson TH. Numerical simulation for the design analysis of kinematic Stirling engines. Appl Energy 2015;159.

doi:10.1016/j.apenergy.2015.09.024.

[18] Ahmadi MH, Ahmadi MA, Pourfayaz F. Thermal models for analysis of performance of Stirling engine: A review. Renew Sustain Energy Rev 2017;68:168–84. doi:10.1016/j.rser.2016.09.033.

[19] Hachem H, Gheith R, Aloui F, Ben Nasrallah S. Technological challenges and optimization efforts of the Stirling machine: A review. Energy Convers Manag 2018;171:1365–87. doi:10.1016/j.enconman.2018.06.042.

[20] Izadiamoli N, Sayyaadi H. Conceptual design, optimization, and assessment of a hybrid Otto-Stirling engine/cooler for recovering the thermal energy of the exhaust gasses for automotive applications. Energy Convers Manag 2018;171:1063–82. doi:10.1016/j.enconman.2018.06.056.

[21] Beale WT, Wood JG, Chagnot BF. Stirling engine for developing countries. Am Inst Aeronaut Astronaut 1980.

[22] Kongtragool B, Wongwises S. Investigation on power output of the gamma-configuration low temperature differential Stirling engines. Renew Energy 2005;30:465–76. doi:10.1016/j.renene.2004.06.003.

[23] Kongtragool B, Wongwises S. Investigation on power output of the gamma-configuration low temperature differential Stirling engines. Renew Energy 2005. doi:10.1016/j.renene.2004.06.003.

[24] Egas J. Stirling Engine Configuration Selection. Energies 2018:1–22. doi:10.3390/en11030584.

[25] Gedeon D, Wood JG. Oscillating flow regenerator test rig: hardware and theory with derived correlations for screens and felts 1996.

[26] Walker G. Elementary design guidelines for Stirling engines. Proc. 14th Intersoc. Energy Convers. Eng. Conf., 1979.

[27] Schmidt G. Theorie der Lehmannschen calorischen Maschine. Zeitschrift des Vereines Deutscher Ingenieure 1871;15:97–112.

[28] Martini W. Stirling Engine Design Manual Conservation and Renewable Energy. Methods 1983:412.

[29] Cheng CH, Yang HS. Optimization of geometrical parameters for Stirling engines based on theoretical analysis. Appl Energy 2012;92:395–405. doi:10.1016/j.apenergy.2011.11.046.

[30] Dai D, Liu Z, Yuan F, Long R, Liu W. Finite time thermodynamic analysis of a solar duplex Stirling refrigerator. Appl Therm Eng 2019;156:597–605.

doi:10.1016/j.applthermaleng.2019.04.098.

[31] Chen CL, Ho CE, Yau HT. Performance analysis and optimization of a solar powered stirling engine with heat transfer considerations. Energies 2012;5:3573–85. doi:10.3390/en5093573.

[32] Ahmadi MH, Ahmadi MA, Pourfayaz F, Bidi M, Hosseinzade H, Feidt M. Optimization of powered Stirling heat engine with finite speed thermodynamics. Energy Convers Manag 2016;108:96–105. doi:10.1016/j.enconman.2015.11.005.

[33] Costea M, Petrescu S, Harman C. Effect of irreversibilities on solar Stirling engine cycle performance. Energy Convers Manag 1999;40:1723–31. doi:10.1016/S0196-8904(99)00065-5.

[34] Petrescu S, Costea M, Harman C, Florea T. Application of the direct method to irreversibile Stirling cycles with finite speed. Int J Energy Res 2002;26:589–609.

[35] Petrescu S, Costea M. Development of thermodynamics with finite speed and direct method. Ed AGIR 2011.

[36] Hosseinzade H, Sayyaadi H, Babaelahi M. A new closed-form analytical thermal model for simulating Stirling engines based on polytropic-finite speed thermodynamics. Energy Convers Manag 2015;90:395–408. doi:10.1016/j.enconman.2014.11.043.

[37] Chahartaghi M, Sheykhi M. Thermal modeling of a trigeneration system based on beta-type Stirling engine for reductions of fuel consumption and pollutant emission. J Clean Prod 2018;205:145–62. doi:10.1016/j.jclepro.2018.09.008.

[38] Finkelstein T. Thermodynamic analysis of Stirling engines. J Spacecr Rocket 1967;4:1–9.

[39] Urieli I, Berchowitz D. Stirling cyle engine analysis. Adam Hilger LTD 1984.

[40] Ã YT, Tlili I, Nasrallah S Ben. Design and performance optimization of GPU-3 Stirling engines. Energy 2008;33:1100–14. doi:10.1016/j.energy.2008.02.005.

[41] Babaelahi M, Sayyaadi H. Simple-II: A new numerical thermal model for predicting thermal performance of Stirling engines. Energy 2014;69:873–90. doi:10.1016/j.energy.2014.03.084.

[42] Babaelahi M, Sayyaadi H. A new thermal model based on polytropic numerical simulation of Stirling engines. Appl Energy 2015;141:143–59. doi:10.1016/j.apenergy.2014.12.033.

[43] Babaelahi M, Sayyaadi H. Modified PSVL: A second order model for thermal simulation of Stirling engines based on convective-polytropic heat transfer of working spaces. Appl Therm Eng 2015;85:340–55. doi:10.1016/j.applthermaleng.2015.03.018.

[44] Araoz JA, Salomon M, Alejo L, Fransson TH. Non-ideal Stirling engine thermodynamic model suitable for the integration into overall energy systems. Appl Therm Eng 2014;73:203–19. doi:10.1016/j.applthermaleng.2014.07.050.

[45] Chahartaghi M, Sheykhi M. Energy and exergy analyses of beta-type Stirling engine at different working conditions. Energy Convers Manag 2018;169:279–90. doi:10.1016/j.enconman.2018.05.064.

[46] Cheng CH, Yang HS, Keong L. Theoretical and experimental study of a 300-W beta-type Stirling engine. Energy 2013;59:590–9. doi:10.1016/j.energy.2013.06.060.

[47] Yang HS, Cheng CH, Huang ST. A complete model for dynamic simulation of a 1-kW class beta-type Stirling engine with rhombic-drive mechanism. Energy 2018;161:892–906. doi:10.1016/j.energy.2018.07.159.

[48] Hosseinzade H, Sayyaadi H. CAFS: The Combined Adiabatic-Finite Speed thermal model for simulation and optimization of Stirling engines. Energy Convers Manag 2015;91:32–53. doi:10.1016/j.enconman.2014.11.049.

[49] Sheykhi M, Chahartaghi M, Balakheli MM, Kharkeshi BA, Miri SM. Energy, exergy, environmental, and economic modeling of combined cooling, heating and power system with Stirling engine and absorption chiller. Energy Convers Manag 2019. doi:10.1016/j.enconman.2018.10.102.

[50] Sayyaadi H, Ghasemi H. A novel second-order thermal model of Stirling engines with consideration of losses due to the speed of the crack system. Energy Convers Manag 2018. doi:10.1016/j.enconman.2018.05.021.

[51] Li R, Grosu L, Li W. New polytropic model to predict the performance of beta and gamma type Stirling engine. Energy 2017;128:62–76. doi:10.1016/j.energy.2017.04.001.

[52] El-Ghafour SA, El-Ghandour M, Mikhael NN. Three-dimensional computational fluid dynamics simulation of stirling engine. Energy Convers Manag 2019;180:533–49. doi:10.1016/j.enconman.2018.10.103.

[53] Toghyani S, Kasaeian A, Hashemabadi SH, Salimi M. Multi-objective optimization of GPU3 Stirling engine using third order analysis. Energy Convers Manag 2014;87:521–9. doi:10.1016/j.enconman.2014.06.066.

[54] Jan W, Marek P. Mathematical Modeling of the Stirling Engine. Procedia Eng 2016;157:349–56. doi:10.1016/j.proeng.2016.08.376.

[55] Mohammadi MA, Jafarian A. CFD simulation to investigate hydrodynamics of oscillating flow in a beta-type Stirling engine. Energy 2018;153:287–300.

doi:10.1016/j.energy.2018.04.017.

[56] Almajri AK, Mahmoud S, Al-Dadah R. Modelling and parametric study of an efficient Alpha type Stirling engine performance based on 3D CFD analysis. Energy Convers Manag 2017;145:93–106. doi:10.1016/j.enconman.2017.04.073.

[57] Xiao G, Sultan U, Ni M, Peng H, Zhou X, Wang S, et al. Design optimization with computational fluid dynamic analysis of β-type Stirling engine. Appl Therm Eng 2017;113:87–102. doi:10.1016/j.applthermaleng.2016.10.063.

[58] Abuelyamen A, Ben-Mansour R. Energy efficiency comparison of Stirling engine types (α, β, and γ) using detailed CFD modeling. Int J Therm Sci 2018;132:411–23. doi:10.1016/j.ijthermalsci.2018.06.026.

[59] Abuelyamen A, Ben-Mansour R, Abualhamayel H, Mokheimer EMA. Parametric study on beta-type Stirling engine. Energy Convers Manag 2017;145:53–63. doi:10.1016/j.enconman.2017.04.098.

[60] Alfarawi S, AL-Dadah R, Mahmoud S. Influence of phase angle and dead volume on gamma-type Stirling engine power using CFD simulation. Energy Convers Manag 2016;124:130–40. doi:10.1016/j.enconman.2016.07.016.

[61] Buliński Z, Kabaj A, Krysiński T, Szczygieł I, Stanek W, Rutczyk B, et al. A Computational Fluid Dynamics analysis of the influence of the regenerator on the performance of the cold Stirling engine at different working conditions. Energy Convers Manag 2019;195:125–38. doi:10.1016/j.enconman.2019.04.089.

[62] Homutescu VM, Dumitrascu G, Horbaniuc B. Evaluation of the work lost due to leaks through cylinder-displacer gap 2008.

[63] Ahmed F, Hulin H, Khan AM. Numerical modeling and optimization of beta-type Stirling engine. Appl Therm Eng 2019;149:385–400. doi:10.1016/j.applthermaleng.2018.12.003.

[64] Kays WM, London AL. Compact Heat Exchangers. Krieger Pub Co.; 1998.

[65] Mabrouk MT, Kheiri A, Feidt M. Effect of leakage losses on the performance of a β type Stirling engine. Energy 2015;88:111–7. doi:10.1016/j.energy.2015.05.075.